การขนส่งโมเลกุลมหภาคในการกรองผ่านโกลเมอร์รูลัส

นายปิยะ พละคช

วิทยานิพนธ์นี้เป็นส่วนหนึ่งของการศึกษาตามหลักสูตรปริญญาวิทยาศาสตรมหาบัณฑิต
สาขาวิชาฟิสิกส์ ภาควิชาฟิสิกส์
คณะวิทยาศาสตร์ จุฬาลงกรณ์มหาวิทยาลัย
ปีการศึกษา 2555

TRANSPORT OF MACROMOLECULES IN GLOMERULAR FILTRATION

Mr. Piya Phalakhoj

A Thesis Submitted in Partial Fulfillment of the Requirements
for the Degree of Master of Science Program in Physics
Department of Physics
Faculty of Science
Chulalongkorn University
Academic Year 2012

Thesis Title	TRANSPORT OF MACROMOLECULES IN GLOMERULAR FILTRATION
By	Mr. Piya Phalakhoj
Department	Physics
Thesis Advisor	Panadda Dechadilok, Ph.D.

Accepted by the Faculty of Science, Chulalongkorn University in Partial Fulfillment of the Requirements for the Master ’s Degree

……Dean of Faculty of Science
(Professor Supot Hannongbua, Dr. rer. nat.)

THESIS COMMITTEE

……Chairman
(Associate Professor Mayuree Natenapit, Ph.D.)

……Thesis Advisor
(Panadda Dechadilok, Ph.D.)

……Examiner
(Chatchai Srinitiwarawong, Ph.D.)

……..…External Examiner
(Associate Professor Wannapong Triampo, Ph.D.)

ปิยะ พละคช : การขนส่งโมเลกุลมหภาคในการกรองผ่านโกลเมอร์รูลัส (TRANSPORT OF MACROMOLECULES IN GLOMERULAR FILTRATION) อ. ที่ปรึกษาวิทยานิพนธ์หลัก: อ.ดร.ปนัดดา เดชาดิลก, 66 หน้า.

หน้าที่หลักของไต คือ การกรองเลือดโดยรักษาไว้ซึ่งองค์ประกอบและปริมาตรของเลือด กระบวนการกรองเกิดขึ้นในชั้นแรกบริเวณผนังโกลเมอร์รูลา คาพิลลารี ซึ่งประกอบด้วยเนื้อเยื่อ 3 ชั้น ได้แก่ ชั้นเอนโดทีเลียม, โกลเมอร์รูลา เบสเมนต์ เมมเบรน (จีบีเอ็ม) และชั้นอีพิทีเลียล ซึ่งประกอบด้วยฟุตโพรเซสที่ถูกเชื่อมไว้ด้วยสลิตไดอะเฟรม งานวิจัยนี้มุ่งศึกษาการขนส่งโมเลกุลไมโอโกลบิน ซึ่งเป็นตัวบ่งชี้ทางชีวภาพสำหรับความเสียหายที่เกิดขึ้นกับกล้ามเนื้อและเป็นสาเหตุหนึ่งของโรคไตวายเฉียบพลัน แบบจำลองทางอุทกพลศาสตร์ถูกสร้างขึ้นเพื่ออธิบายการขนส่งโมเลกุลมหภาคซึ่งเป็นกลางทางไฟฟ้าเคลื่อนที่ผ่านสลิตไดอะเฟรมและจีบีเอ็ม สลิตไดอะเฟรมถูกจำลองให้เป็นแถวของไฟเบอร์ทรงกระบอกขนาน ในขณะที่จีบีเอ็มถูกกำหนดให้เป็นตัวกลางเนื้อเดียวที่ประกอบด้วยไฟเบอร์ไขว้กันไปมา ผลการคำนวณเชิงตัวเลขของค่าสัมประสิทธิ์การกรองของไมโอโกลบินซึ่งเป็นผลคูณระหว่างค่าสัมประสิทธิ์การกรองของสลิตไดอะเฟรมและจีบีเอ็มสอดคล้องกับค่าสัมประสิทธิ์การกรองซึ่งได้จากการนับจำนวนกัมมันตภาพรังสีของไมโอโกลบินที่ถูกย้อมด้วยรังสีในกระแสเลือดและปัสสาวะ หากว่าในการคำนวณกำหนดให้จีบีเอ็มมีไฟเบอร์ขนาดรัศมีเป็น 0.5 นาโนเมตรเท่านั้น (โดยไม่คำนึงถึงว่าในจีบีเอ็มมีไฟเบอร์ของคอลลาเจนไทป์โฟร์ประกอบอยู่ด้วย) และหากกำหนดให้ขนาดของที่ว่างระหว่างไฟเบอร์ในสลิตไดอะเฟรมมีค่าประมาณ 10 นาโนเมตร เมื่อทำการคำนวณโดยไม่คิดผลจากสลิตไดอะเฟรมค่าสัมประสิทธิ์การกรองรวมเพิ่มขึ้นเพียง 6-7% จึงสามารถสรุปได้ว่าจีบีเอ็มน่าจะมีส่วนสำคัญต่อการกรองไมโอโกลบินของโกลเมอร์รูลัส แต่ยังไม่สามารถสรุปได้ว่าสลิตไดอะเฟรมไม่มีส่วนต่อการกรอง เนื่องจากการกำหนดขนาดของที่ว่างระหว่างไฟเบอร์ในสลิตไดอะเฟรมเท่ากับ10 นาโนเมตรนั้นเป็นค่าขอบเขตสูงสุด ความเข้าใจเกี่ยวกับสัดส่วนการกรองของแต่ละชั้นจึงยังคงต้องการการตรวจสอบเพิ่มมากขึ้น

ภาควิชา ฟิสิกส์ ลายมือชื่อนิสิต .....

สาขาวิชา ฟิสิกส์ ลายมือชื่อ อ.ที่ปรึกษาวิทยานิพนธ์หลัก.....

ปีการศึกษา 2555

5272426123 : MAJOR PHYSICS
KEYWORDS : HINDERED TRANSPORT/ MACRAMOLECULES/ SINGLE ROW OF CYLINDERS/ PARALLEL FIBERS

PIYA PHALAKHOJ: TRANSPORT OF MACROMOLECULES IN GLOMERULAR FILTRATION. ADVISOR : PANADDA DECHADILOK, Ph.D., 66 pp.

The main function of kidneys is to retain the normal blood composition and volume through blood filtration: the first step of which occurs at the glomerular capillary wall that consists of three layers: the endothelium cell layer, the glomerular basement membrane (GBM) and the epithelial foot processes with their interconnecting slit diaphragm. Our research focuses on the transport of myoglobin, a biomarker for muscle damage and one of the causes of acute renal failure. A hydrodynamic model is introduced to describe hindered transport of electrically-neutral macromolecules through the epithelial slit and a glomerular basement membrane (GBM). The slit diaphragm is modeled as a row of parallel cylindrical fibers and the GBM is treated as an isotropic fibrous medium. Numerically calculated sieving coefficient of myoglobin, a product of the sieving coefficient of the slit diaphragm and that of the GBM, is found to be in good agreement with sieving coefficient obtained from counting radioactivity of radiolabeled myoglobins in blood and urine, if, in the calculation, GBM fiber radii are assumed to be 0.5 nm (with the presence of type IV collagen in the GBM neglected). With the gap between adjacent fibers in the epithelial slit diaphragm (L) assumed to be about 10 nm, the absence of the slit diaphragm increases the sieving coefficient by only 6-7%. It seems that the GBM contributes significantly to the restriction of myoglobin in glomerular filtration, although it might still be too early to say that the contribution of slit diaphragm is negligible, given that the values of L = 10 nm is the upper limit. Further investigation is needed to fully understand the contribution of each layer.

Department : Physics Student's Signature .....
Field of Study : Physics Advisor's Signature .....
Academic Year : 2012

ACKNOWLEDGEMENTS

After a long time, my thesis is finally completed. First, I would like to express my deepest gratitude to my advisor Dr. Panadda Dechadilok for her suggestions, keen interest and encouragement as well as for valuable guidance in dealing with simulation work.

I also would like to thank Assoc. Prof. Dr. Mayuree Natenapit, Assoc. Prof. Dr. Wannapong Triampo and Dr. Chatchai Srinitiwarawong for taking the time from their busy schedules to be on my thesis committee. Their comments on this thesis are also greatly appreciated. I also would like to express my gratitude to Asst. Prof. Dr. Kajornyod Yoodee for his helpful suggestions, Thanks Asst. Prof. Dr. Sakuntam Sanorpim and Asst. Prof. Dr. Tonphong Kaewkongka for their kindness in letting me share their laboratory.

I want to thanks to Miss Waranya Jampamoon for her help in checking my thesis format and for encouraging me in such a difficult time. Love and support from my family and all my friends are deeply appreciated.

I also would like to thank The Institute for the Promotion of Teaching Science and Technology (IPST) for granting me a financial support support from high school to graduate school, and Khanom Pitaya School for allowing me to take a leave of absence to finish my master's degree.

Finally, a financial support from Faculty of Science, Chulalongkorn University and The Thai Research Fund in completing this thesis is greatly appreciated.

CONTENTS

Page

LIST OF TABLES

LIST OF FIGURES

Figures Page

Figures Page

Figures Page

CHAPTER I
INTRODUCTION

The main function of human kidney is to filter blood, remove excess proteins and metabolic waste while retaining the normal blood composition and blood volume. The first step of blood filtration occurs at the glomerular capillary walls within a nephron shown in Fig. 1.1. Inside the nephron, the glomerulus, a network of blood capillary, is surrounded by Bowman's capsule containing urine. Excess fluid, proteins and metabolic wastes are transported from the blood stream through the glomerular capillary wall into primary urine in Bowman's capsule. The glomerular capillary wall is normally very permeable to water, allowing non-restricted passage of small and middle-sized molecules, while restricting passage of macromolecules such as serum albumin [1]. It is desired to relate nanostructure of each layer of glomerular capillary wall as well as basic properties of macromolecules such as size, charge, and shape, to measurable quantities such as rate of water transport and sieving coefficient (a ratio between upstream and downstream concentration) of macromolecules.

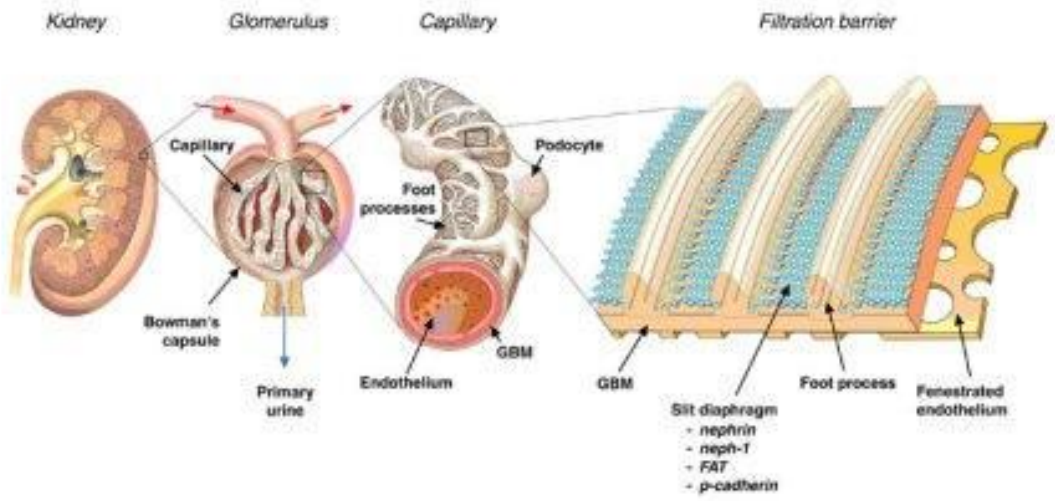

Figure 1.1 Schematic view of a kidney, a glomerulus and a glomerular capillary wall. [2]

1.1 Overview of Glomerular Filtration

As shown in Figs. 1.2 and 1.3, the glomerular capillary wall is one of the most complex biological membrane, consisting of multiple cellular layers: an endothelial cell layer (the inner most layer), a glomerular basement membrane (GBM) and an epithelial cells layer (the outer most layer next to Bowman's capsule). The filtration pathway is demonstrated by the arrows. Fluid and macromolecules enter the glomerular capillary wall through the endothelial fenestrae. After that, they are transported across the GBM into the primary urine in Bowman's capsule through the slit diaphragm connected to the epithelial podocytes.

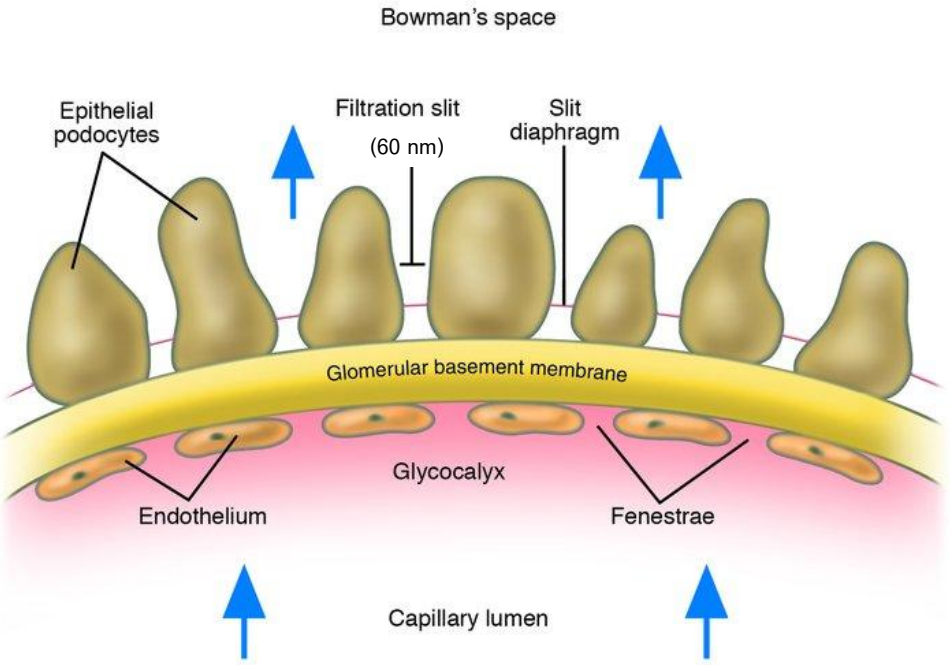

Figure 1.2 Structure of glomerular capillary wall with different cellular layers: a fenestrated endothelium cell layer, a glomerular basement membrane (GBM), and the epithelial foot processes [3]. Figure is not drawn to scale. Arrows indicate the transport direction of the macromolecules from within the capillary lumen to Bowman's capsule.

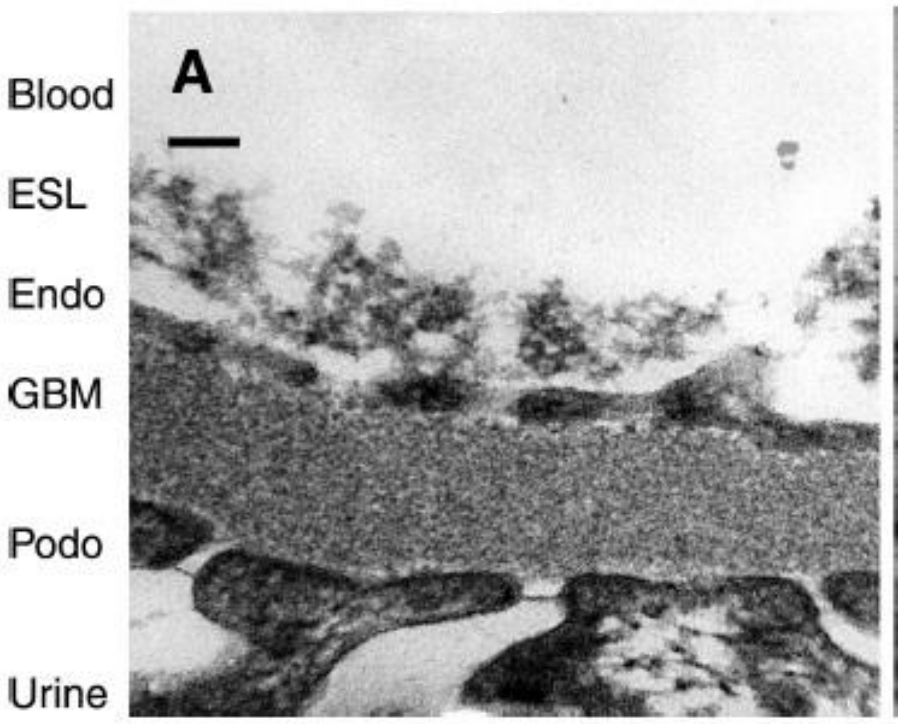

Figure 1.3 Electron micrograph of glomerular capillary wall with the capillary lumen above and the urinary space below. Scale bar = 100 nm [1]

The inner most layer, the glomerular endothelial cell layer, is the cellular layer lining the capillary lumen in contact with blood stream. Approximately 20-50% of the endothelial surface area are covered with large round or oval-like shaped fenestrates. The electron micrograph scanning reported that the diameter of the fenestrae are about 60 nm [1], much larger than plasma proteins such as albumins with radii about 3.6 nm or myoglobins with radii about 2 nm. Although the fenestrae are too large to contribute to the size-selectivity of the glomerular barrier, it does contribute to the charge-selectivity of the glomerular capillary wall due to the fact that the endothelial cell surface has negatively charge proteoglycans.

The middle layer, glomerular basement membrane (GBM), is a hydrogel believed to be 90-93% water by volume [4] and composed of a fibrous network consisting of typeIV collagen and proteoglycan as well as other protein fibers such as

laminin and nidogen/entactin [1]. In the past, researchers assumed that the glomerular basement membrane, the thickest layer (with a thickness of approximately 240-370 nm), was the most selective layer. but in vitro ultrafiltration through isolated GBM suggested that, although the GBM may contribute to restriction of solute transport, other cellular layers is likely to also play a crucial role in maintaining glomerular selectivity [5,6]. Mutations in the collagen chains within the GBM create a severe pathological conditions: the most well-known being Alport's syndrome.

The outer most layer, the epithelial cell layer, is believed to be a major barrier restricting the passage of macromolecules [7, 8]. This cellular layer lines the outside of the glomerular barrier, facing the Bowman's capsule containing primary urine. The cells have long extending cytoplasmic foot processes, separated by a filtration slit that is about 25-60 nm [1] and covered by a diaphragm, as shown in Fig. 1.4. An electron microscopic study showed that the slit diaphragm has a unique structure consisting of planar arrangement of fibers resulting in space allowing a passage of molecules with dimensions previously postulated to be 4x14 nm [9]. However, several experiments have shown that even proteins with radii as large as 3.6 nm can still pass through the glomerular capillary wall. Recent electron micrograph gave an estimate of the width of spaces between fibers of glomerular slit diaphragm to be 4-20 nm.

We are particularly interested in transport of myoglobins through glomerular barrier. Myoglobin is considered to be the oxygen tank of the tissue muscle, being the primary oxygen-carrying pigment, and is a sensitive bio-marker for muscle injury. Myoglobinuria, a symptom of having excessive amount of myoglobin in urine, is often associated with rhabdomyolysis or muscle destruction. Damaged muscle releases myoglobin which is then filtered by the kidney but is toxic to the renal tubular epithelium, capable of causing an acute renal failure. We are, therefore, interested in relating quantities that can be measured experimentally such as sieving coefficient of myoglobin (discussed below) to cellular structures of the glomerular capillary wall. Stokes-Einstein radii of myoglobins are about 2 nm, and they are globular proteins which means that their shapes are relatively spherical. To make the procedure simpler, the scope of this research is restricted to electrically-neutral myoglobins such as nMyoglobin.

Table 1.1 Parameter values for transport of macromolecules through slit diaphragm.

Parameter	Values
Slit diaphragm width	25 - 60 nm
Distance from GBM to slit diaphragm ($L_{\text{GBM-Slit}}$)	30 - 70 nm
Fibers radii (R)	2-10 nm
The width of spaces between fibers	4 - 20 nm
An average velocity in the epithelial slit.	3 x 10^{-5} m/s
A pressure drop in the epithelial slit.	3.8 x 10^{2} Pa
Myoglobins radii (r_s)	2 nm

1.2 Overall Sieving Coefficient

The objective of this thesis is to relate quantities that can be measured experimentally to nanostructures of the glomerular capillary wall. One of such quantities is a solute sieving coefficient: a ratio between upstream solute concentration in the capillary lumen (C_P) and downstream solute concentration in Bowman's capsule (C_B):

$$\theta = \frac{C_B}{C_P} \qquad (1.1)$$

The overall sieving coefficient (θ) of the glomerular capillary wall is the product of sieving coefficient of the three cellular layers:

$$\theta = \theta_{en}\theta_{bm}\theta_{SD}. \qquad (1.2)$$

where θ_{en}, θ_{bm} and θ_{SD} are the sieving coefficients of the fenestrated endothelium, the basement membrane and the epithelium (slit diaphragm) respectively. However, because we focus on electrically-neutral molecules and because a fenestrated opening

in the endothelial cell layer is large (~30 nm in radius) compared with the radius of myoglobin (r_s ~ 2 nm), $\theta_{en} \approx 1$ resulting in the overall sieving coefficient of the glomerular barrier being simply the product between sieving coefficients of the GBM and the epithelial slit diaphragm as shown below:

$$\theta \cong \theta_{bm}\theta_{SD}. \tag{1.3}$$

The solute sieving coefficient for the epithelial slit is defined as following:

$$\theta_{SD} = \frac{C_B}{C_0} \tag{1.4}$$

where C_0 is the average solute concentration of the upstream flow at the GBM-epithelium interface and C_B is the average solute concentration in Bowman's space. θ_{bm} is the sieving coefficient for the GBM defined as following:

$$\theta_{bm} = \frac{C_0}{C_P} \tag{1.5}$$

1.3. Overview of Mathematical Model Development

Shown in Fig. 1.4 is the idealized structural unit of the glomerular capillary wall, where the width of the structural unit (W) is 360 nm and the thickness of GBM (H) is about 200-400 nm. The distance between the epithelial podocytes is 25-60 nm. As evident from Eq. (1.3), in order to calculate the overall glomerular sieving coefficient, sieving coefficients of solutes across the GBM and through the epithelial slit must be first determined. A mathematical model is developed to explain transport of macromolecules through both layers. A slit diaphragm is modeled as a row of parallel cylindrical fibers as suggested by Hora et al.[11] as well as by Drumond and Deen [12]. GBM is modeled as an isotropic hydrogel with randomly oriented cylindrical fibers. A comparison between our calculated overall sieving coefficient and data from experiment employing the tissue-uptake technique [13] will be made.

The purpose of this work is to determine how each layer, namely the GBM and the epithelial slit, contributes to the overall sieving coefficient of electrically-neutral and spherical macromolecules with sizes comparable to myoglobin. In other words, we would like to investigate which glomerular layer is likely to contribute most to the restriction of myoglobin.

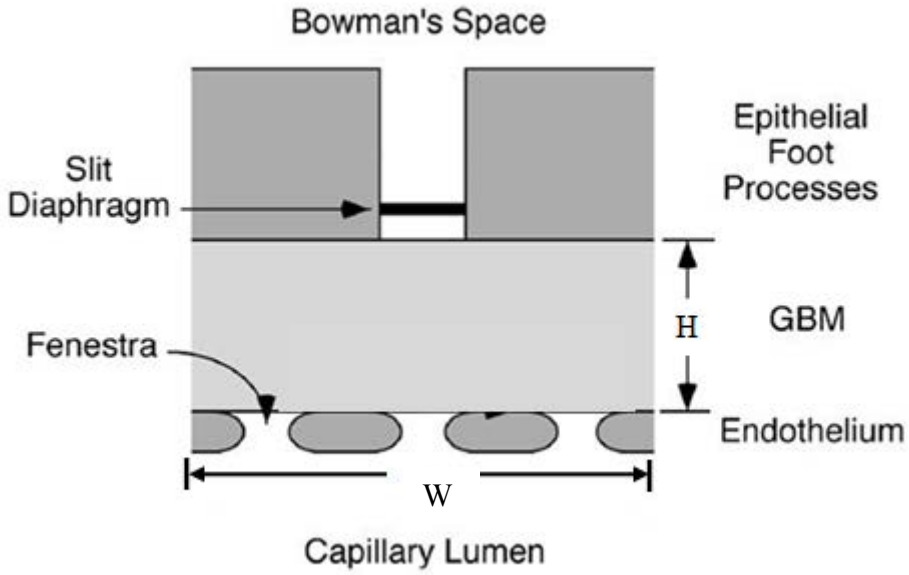

Figure 1.4 depicts the idealized structural unit of the glomerular capillary wall. W is the width of the unit (360 nm), while H is the thickness of the glomerular basement membrane (on the order of 200-400 nm).

CHAPTER II

HINDERED DIFFUSION THROUGH A SLIT DIAPHRAGM

As mention in chapter 1, the epithelial cell layer, is the outer most layer of the glomerular barrier in contact with the primary urine. The epithelial cells have long extending cytoplasmic foot processes, separated by a filtration slit that is about 25-60 nm [1] and covered by a diaphragm, as shown in Fig. 2.1A. Fig. 2.1B is a top-view electron microscopic study showing that the slit diaphragm has a unique structure consisting of planar arrangement of fibers resulting in space allowing a passage of molecules : recent electron micrograph gives an estimate of the width of spaces between fibers of glomerular slit diaphragm to be 4-20 nm. Clinical investigation demonstrated that mutation of the nephrin gene causes a change in slit diaphragm structure leading to congenital nephrotic syndrome of the Finnish type of which one of the symptoms is a massive leakage of proteins into urine (proteinuria).

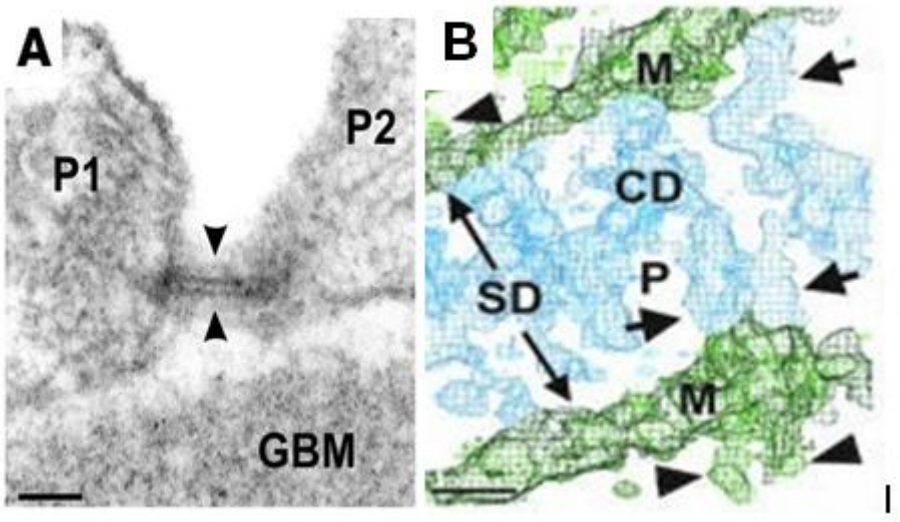

Figure 2.1 Electron microscopic showing both side-view (2.1A) and top-view (2.1B) images of the epithelial slit diaphragm. Scale bar: 40 nm (A) and 10 nm (B) [10].

Fig. 2.2A is the idealized schematic drawing of a slit diaphragm connecting two epithelial podocytes. To describe transport of water and molecules through the

glomerular slit diaphragm, Rodewald and Karnovsky proposed a "zipper" configuration, shown in Fig. 2.2B, with a central filament connecting foot processes by alternating cross-bridges on either side. Hora et al.[[11] and Drumond and Deen [12] proposed an alternative "ladder" structure, with a row of fibers connecting the foot processes and spanning the entire slit, shown in Fig. 2.2C. In this thesis, the glomerular slit diaphragm is modeled as a "ladder" structure, based on the observations of Hora et al.[11].

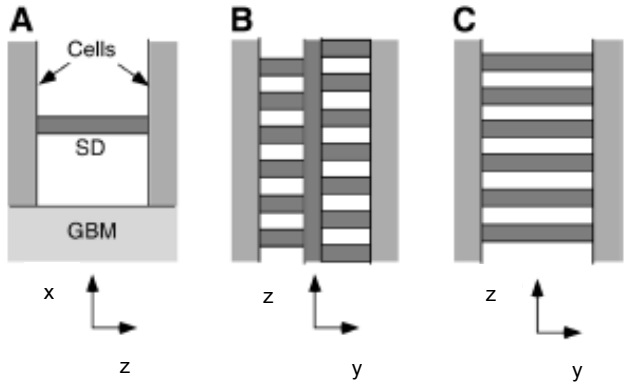

Figure 2.2 A: Representations of the epithelial slit diaphragm (SD). B: zipper configuration. C: ladder configuration [13].

The macromolecule is assumed to be a rigid electrically-neutral sphere passing through a row of infinitely-long parallel cylindrical fibers, as shown in Fig. 2.3. Up until now, there have been theoretical studies on enhanced drag and hindered diffusion due to a presence of a plane wall [14,15], as well as hindered diffusion in cylindrical and slit pores [16, 17]. Investigations on hindered diffusion in fibrous membranes [18,19] and hydrogel [20] have also been done. However, a study on hindered diffusion of a particle moving through a row of parallel fibers remained largely absent, except for a theoretical calculation performed by Drumond and Deen [12], where the hydrodynamic resistance was approximated using the enhanced drag of a sphere moving between parallel plates [21].

This chapter focuses on hindered diffusion of a rigid and uncharged spherical solute moving through a row of parallel fibers. First, the solute flux in an unbounded

fluid will be introduced. Then, the force coefficient tensors as well as the diffusive hindrance factor tensor in the solute flux will be defined. The solute is assumed to be moving slowly such that the Reynolds number is small. The numerical results for force coefficients obtained from simulations employing finite element method as well as lubrication theory, and the diffusive hindrance factors will be presented.

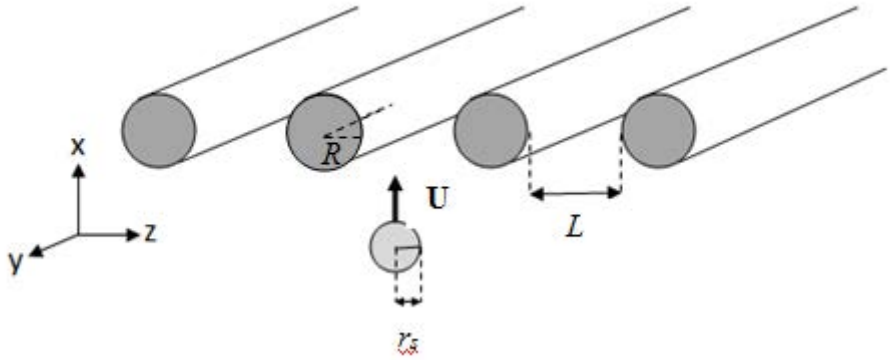

Figure 2.3 Schematic for transport of spherical macromolecules through a row of infinitely long cylinders. R = fiber radius. r_s = sphere radius. L = distance between surface of two adjacent fibers.

2.1 Solute Flux in an Unbounded Fluid

For a particle several times larger than liquid molecules, its motion in liquid solvent can be classified as a Brownian motion. The constitutive equation for a dilute solute flux is derived from balancing the chemical potential gradient per molecule (effective body force) and the hydrodynamic drag, neglecting random fluctuation in solute velocity. If the solute is spherical, this equation can be written as following:

$$-k_B T \ln \nabla C = 6\pi\mu r_s \mathbf{U} \tag{2.1}$$

where k_B is Boltzmann's constant, T is temperature, C is concentration of solute, μ is a fluid viscousity, r_s is a radius of solute and $\mathbf{U}$ is solute velocity. The solute flux, $\mathbf{N}$, relative to a fixed coordinates, defined as

$$\mathbf{N} = \mathbf{U}C \tag{2.2}$$

Combining Eqs. (2.1) and (2.2), the solute flux becomes

$$\mathbf{N} = -D_\infty \nabla C \tag{2.3}$$

D_∞ is the solute diffusivity given by the Stokes-Einstein equation:

$$D_\infty = \frac{k_B T}{6\pi\mu r_s} \tag{2.4}$$

As shown in Eq.(2.4) , the solute diffusivity is the ratio between the thermal fluctuation energy and the hydrodynamic drag coefficient.

2.2 Diffusive Flux through a Slit Diaphragm

In this thesis, the slit diaphragm is modeled as a row of parallel infinitely-long cylindrical fibers. Macromolecule is assumed to be a rigid sphere particle with radius r_s moving with velocity $\mathbf{U}$ through a row of cylinders. The distance between the surface of cylinders is *L* and the cylinder radius is *R* as show in Fig. 2.3.

There are also some additional assumptions. The solution is assumed to be dilute enough such that there is no solute-solute interaction. Sphere radius is much more larger than that of the solvent. Therefore, the solvent is thought as a continuum medium. The hydrodynamic interaction between the solute and the fibers increases the hydrodynamic drag on the solute shown as the parameters $\mathbf{f}$ in the following equation:

$$-kT\nabla \ln C - 6\pi\mu r_s \mathbf{f}\cdot\mathbf{U} = \mathbf{0} \tag{2.5}$$

where $\mathbf{f}$ is a second order force coefficient tensors. The tensor $\mathbf{f}$ contains force coefficients for a sphere moving in a stationary fluid defined as

$$\mathbf{f} = \begin{bmatrix} f_{xx} & f_{xy} & f_{xz} \\ f_{yx} & f_{yy} & f_{yz} \\ f_{zx} & f_{zy} & f_{zz} \end{bmatrix} \tag{2.6}$$

where the component f_{ij} is the enhance drag in the i-direction scaled with the Stokes coefficient $(6\pi\mu r_s)$, for a solute moving in the j-direction. $\mathbf{f}$ is position-dependent, meaning that the values of the force coefficients depend on the particle position relative to the row of fibers. In absence of the row of fibers, $\mathbf{f}$ equals the identity matrix. Combining Eqs.(2.2) and (2.5), the solute flux becomes

$$\mathbf{N} = -D_{\infty}\mathbf{d}\cdot\nabla C \tag{2.7}$$

The diffusive hindrance factor, $\mathbf{d}$, is also a second order tensor related to the force coefficient tensor $\mathbf{f}$ by the following equation:

$$\mathbf{d} = \mathbf{f}^{-1} \tag{2.8}$$

In order to determine the hindrance transport coefficient tensors, $\mathbf{d}$, the force coefficient tensors, $\mathbf{f}$ must be first calculated.

2.3 Coupling between Translational and Rotational Motion

In the previous calculation of Drumond and Deen [12], the force on the particle due to its rotation was neglected, and the enhanced hydrodynamic drag was simply the force on a non-rotating sphere. In our studies, we attempted to verify whether the effect of the coupling between translational and rotational motions are, in fact, negligible.

Taking an advantage of the linearity of the Stokes equation, the force on a particle translating at the velocity **U** and rotating angular velocity $\boldsymbol{\omega}$ can be written as

$$\mathbf{F} = 6\pi\mu r_s \mathbf{f_T} \cdot \mathbf{U} + 6\pi\mu r_s^2 \mathbf{f_R} \cdot \boldsymbol{\omega} \tag{2.9}$$

where $\mathbf{f_T}$ and $\mathbf{f_R}$ are second-order tensors containing the force coefficients due to translational and rotational motions respectively. Containing in the tensor $\mathbf{f_T}$ is the translational force coefficient, $f_{T,ij}$,is a scaled force in the *i*-direction on a non-rotating sphere moving in a *j*-direction. Likewise, the rotational force coefficient, $f_{R,ij}$,is a scaled force in the *i*-direction acting on a non-translating particle rotating with angular velocity in the *j*-direction. Analogously, the torque exerting on the particle translating at the velocity $\mathbf{U}$ and rotating at angular velocity $\boldsymbol{\omega}$ is simply

$$\boldsymbol{\tau} = 8\pi\mu r_s^2 \mathbf{T_T} \cdot \mathbf{U} + 8\pi\mu r_s^3 \mathbf{T_R} \cdot \boldsymbol{\omega} \tag{2.10}$$

where $\mathbf{T_T}$ and $\mathbf{T_R}$ are second-order tensors containing the torque coefficients due to translational and rotational motions respectively. The translational torque coefficient, $T_{T,ij}$, is a scaled torque in the *i*-direction on a non-rotating sphere moving in a *j*-direction. Likewise, the rotational torque coefficient, $T_{R,ij}$, is a scaled torque in the *i*-direction on a non-translating particle rotating with angular velocity in the *j*-direction. All of the force and torque coefficients are independent of $\mathbf{U}$ and $\boldsymbol{\omega}$.

Because the particle is spherical, there is no preferred particle orientation. Due to the fact that the constitutive equation is derived assuming an average over many identical particles, it is assumed that f_{ij} is therefore the enhanced drag on a moving particle that experienced zero torque. It is apparent from Eqs. (2.9) and (2.10) that the enhanced drag acting on a non-rotating sphere is different from that acting on a sphere experiencing zero torque. If the effect of rotation is neglected or in other words, the sphere is assumed not to be rotating, the force coefficient tensor, f, is simply the translational force coefficient tensor, $\mathbf{f_T}$. However, if the "zero torque condition" is assumed, then from Eq. (2.10), the relationship between the translational and angular

velocities becomes

$$r_s \boldsymbol{\omega} = -\mathbf{T}_\mathbf{R}^{-1} \cdot \left(\mathbf{T}_\mathbf{T} \cdot \mathbf{U} \right) \tag{2.11}$$

and, as a result, the force coefficient tensor, $\mathbf{f}$, is simply

$$\mathbf{f} = \mathbf{f}_\mathbf{T} - \mathbf{f}_\mathbf{R} \cdot \mathbf{T}_\mathbf{R}^{-1} \cdot \mathbf{T}_\mathbf{T} \tag{2.12}$$

The effect of the coupling between translational and rotational motions will be further discussed in Section 2.5.

2.4 Calculation of Force Coefficients

In order to obtain the force coefficients discussed above, the velocity field and pressure is first calculated. The velocity and length scales are such that the Reynolds number is small enough to make the Navier-Stokes equation become simply the Stokes equation. The velocity and pressure fields are calculated by solving the Stokes and continuity equation written below :

$$\nabla P = \mu \nabla^2 \mathbf{V} \tag{2.13}$$

$$\nabla \cdot \mathbf{V} = 0 \tag{2.14}$$

where P is the pressure and $\mathbf{V}$ is fluid velocity field. Regarding the boundary conditions, the fluid velocity becomes zero far upstream and downstream as $x \to \pm\infty$, and it also has to satisfy the no-slip boundary conditions at the particle and cylinder surfaces. In the simulations attempting to find the translational force and torque coefficients, the particle is assumed to be moving at a unit translational velocity and not rotating. To obtain the rotational force and torque coefficients, the particle is assumed to be rotating at a unit angular velocity, and its translational motion is absent.

Eqs. (2.13) and (2.14) are solved by using the commercial finite element package, COMSOL Multiphysics (COMSOL, Stockholm, Sweden), operating on a 64-bits work station. Including an infinite number of cylinders in the simulations is impossible due to the number of grids and the computer memory it requires. Instead,

finite numbers of cylinders are added each time until including more fibers changed the hydrodynamic force on the particle by less than 1%.

The preliminary test is performed to verify the accuracy of the simulation. A hydrodynamic drag on a sphere moving inside an infinitely long cylinder is computed as a function of particle sizes, and our numerical results are graphically indistinguishable from the reported analytical result [17]. Example of velocity profile caused by a sphere moving near a row of cylinders is shown in Fig. 2.4. The computed force, as well as the diffusive hindrance factor tensors will be reported in Section 2.5.

For the sphere is located with the distance from the fiber surface less than 20% of the fiber radii, the hydrodynamic drag calculation using COMSOL Multiphysics is proved to be incorrect due to an inability to generate small enough meshes. The force coefficient tensor, f, in that region is then obtained from previous results calculated by using the lubrication approximation, assuming that the hydrodynamic drag experienced by the sphere is mostly due to the shear stress within the tiny gap between the sphere and the cylindrical fiber. Goldman, Cox and Brenner calculated the hydrodynamics force experience by a sphere moving parallel and perpendicular to a solid plane wall [14,22]. Falade and Brenner [23] produced expressions for the force and torque experienced by the sphere moving near an infinitely-long cylinder including effect from the surface curvature of the cylinder.

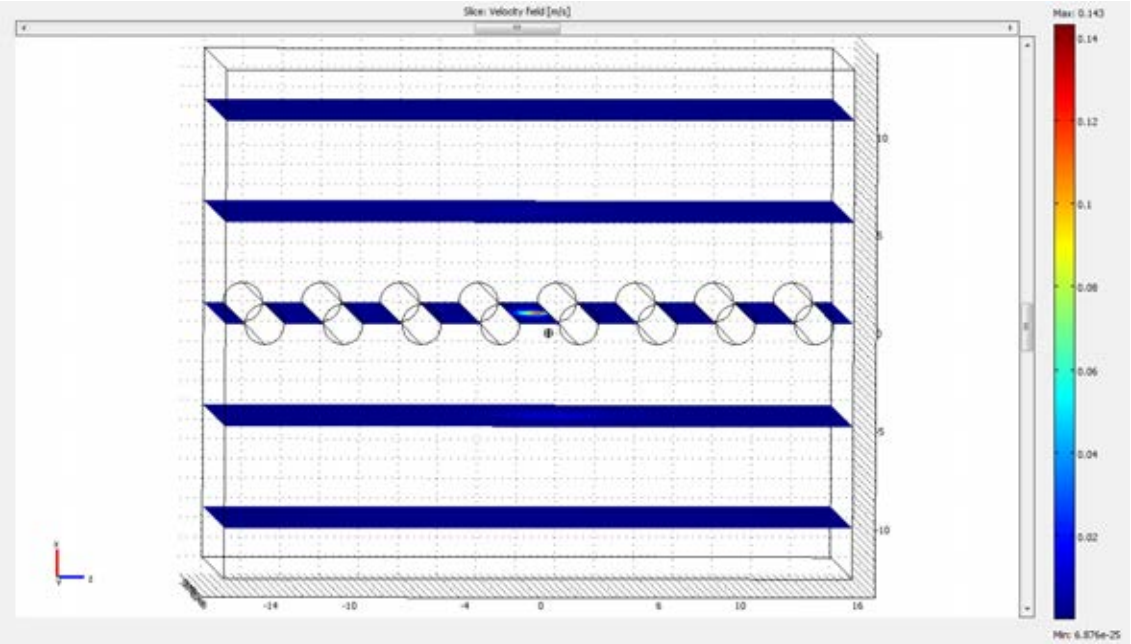

Figure 2.4 Example of velocity profile calculated from solving Stokes' equation using COMSOL Multiphysics. Sphere locate at z/R =0.8, x/R = -1 with r_s/R = 0.2 for $L = 2R$.

In Fig. 2.4, the scale bar on the right show values of the fluid velocity around a moving sphere far from the sphere is at rest while the fluid velocity at the sphere surface equals 1 due to the no-slip boundary condition. A hydrodynamic drag on the sphere is calculated by integrating the pressure and viscous stress over the sphere surface.

2.5 Results and Discussion

Fig. 2.5 and Fig. 2.6 demonstrate the relationship between force coefficients and z/R, defined in Fig. 2.3. Note that having a sphere located at $z = 0$ means that it is located with equal distances from two adjacent fibers. The position $x = 0$ is defined in Fig 2.4. $f_{T,xx}$ is a scaled force in the x-direction on a non-rotating sphere moving in a x-direction and $f_{T,zz}$ is a scaled force in the z-direction on a non-rotating sphere moving in a z-direction, respectively. Results obtained from finite element method

(solid lines) are compared to those obtained by employing lubrication technique by Falade and Brenner (dashed lines). The transition points between the numerical results and lubrication expression were chosen to be the points where the difference between results obtained by the two techniques is less than 1%.

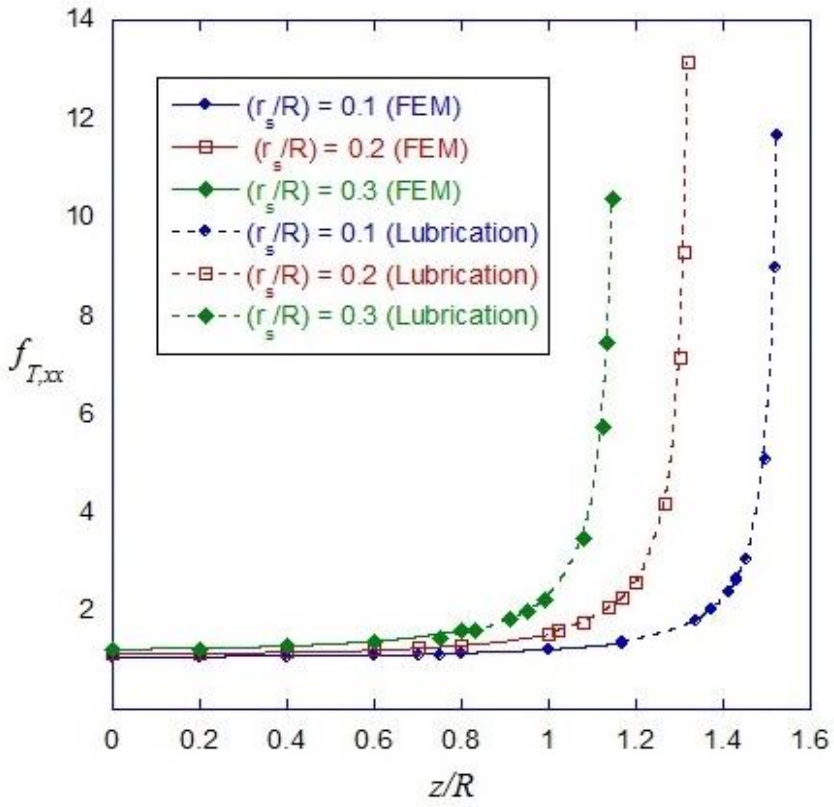

Figure 2.5 Translation force coefficients, $f_{T,xx}$ as a function of z/R at x = -1 (right below a row of fibers). The results were plotted for r_s/R = 0.1, 0.2 and 0.3. $L = 2R$. Solid lines represent results obtained using finite element method. Dashed lines represent the force coefficients obtained from the lubrication expression.

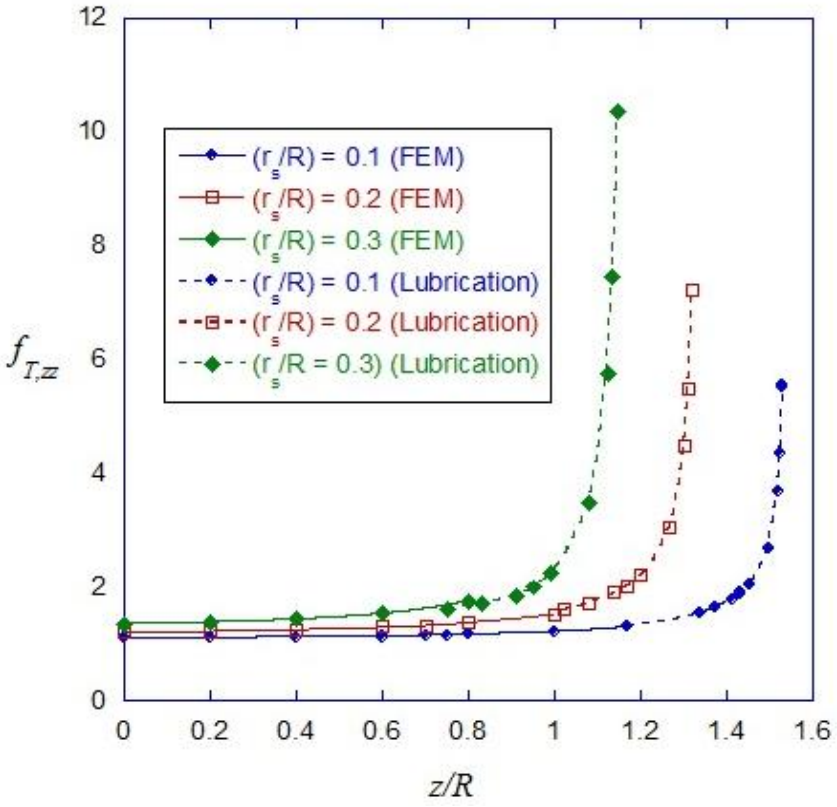

Figure 2.6 Translation force coefficients, $f_{T,zz}$ as a function of z/R at x = -1 (right below a row of fibers). The results were plotted for 3 relative size of the sphere; r_s/R = 0.1, 0.2 and 0.3. $L = 2R$. Solid lines represent the numerical force coefficients. Dashed lines represent the force coefficients from lubrication expression.

As shown in the Fig. 2.5 and Fig. 2.6, an increase in z means a decrease in the distance between the sphere and the fibers. As a result, the sphere-fiber hydrodynamic interaction is enhanced and both $f_{T,xx}$ and $f_{T,zz}$ increase as a function of z. An increase in sphere sizes also result in an increase in $f_{T,xx}$ and $f_{T,zz}$

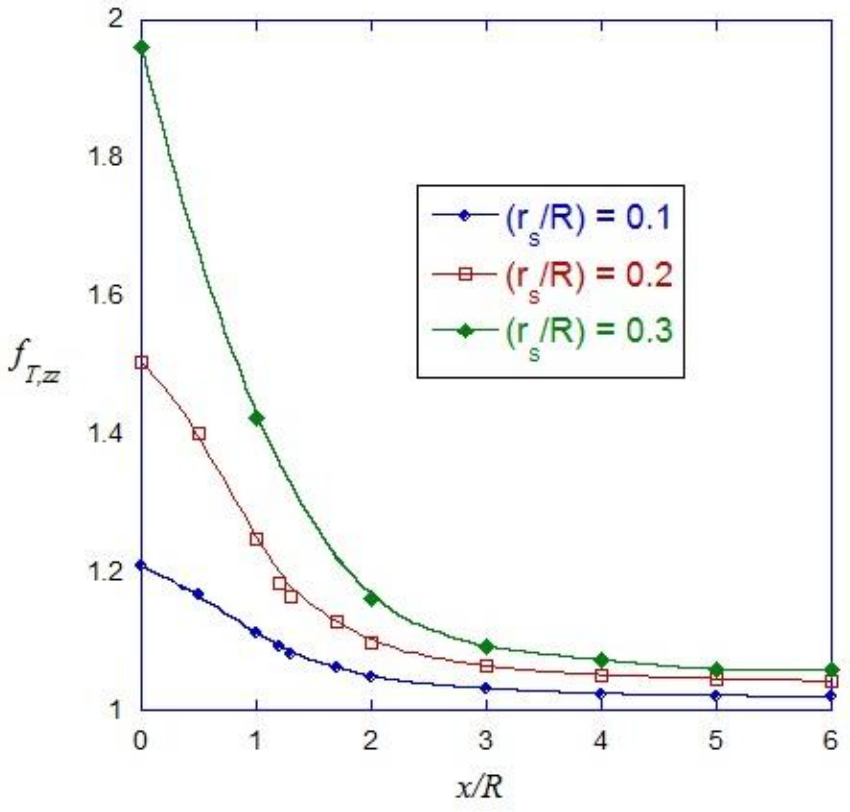

Figure 2.7 Translation force coefficients, $f_{T,zz}$ as a function of x/R at z = 0.4. The results were plotted for 3 relative size of the sphere; r_s/R equals to 0.1, 0.2 and 0.3. $L = 2R$.

As shown in Fig. 2.7, $f_{T,zz}$ is plotted as a function of x/R, a distance between the sphere and the row of fibers. The sphere located at x = 0 would mean that the sphere is located in the closest gap between two adjacent fibers (right in the row of fibers). The enhanced drag acting on the sphere monotonically increases when sphere approaching a row of fibers (or, in other words, as x approaches zero). Once again, the larger the sphere is, the larger the hydrodynamic force it experiences.

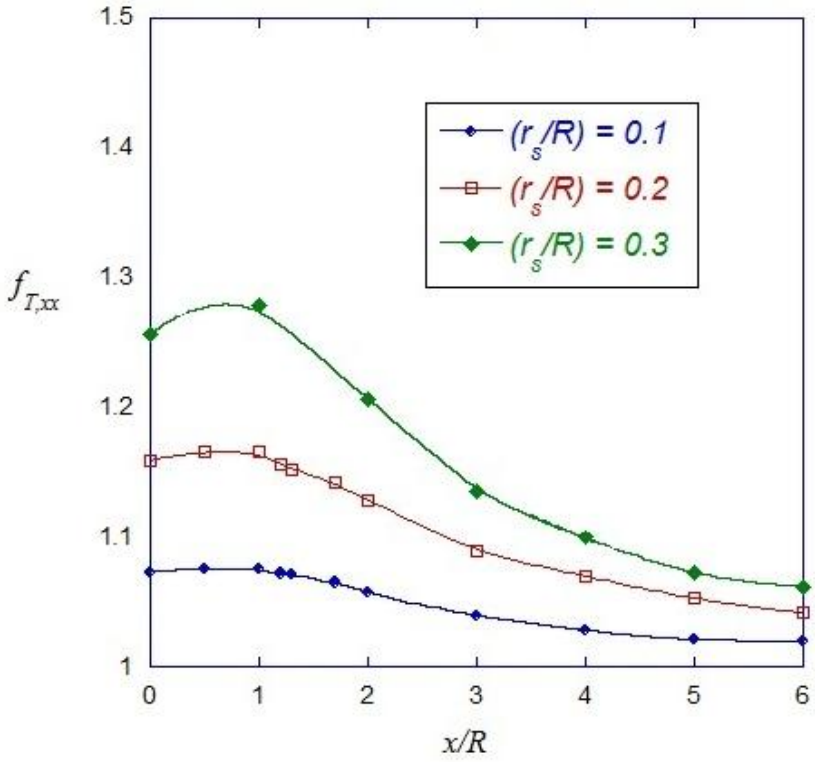

Figure 2.8 Translation force coefficients, $f_{T,xx}$ as a function of x/R at z = 0.4. The results were plotted for 3 relative size of the sphere; r_s/R equals to 0.1, 0.2 and 0.3. $L = 2R$.

Fig. 2.8 presents $f_{T,xx}$ as a function of x/R for three particle sizes. Unlike the monotonic increase of $f_{T,zz}$, $f_{T,xx}$ shows an maximum value at |x| = R, before exhibiting a decrease. This maximum point in the profile of $f_{T,zz}$ was not seen in the previous work by Drumond and Deen [12], where the force coefficients were approximated using the enhanced drag on a sphere between parallel plates. At this point we stipulate that this effect might be caused by the hydrodynamic solute-cylinder interaction. A particle position being at x = 0 would mean that the sphere is located between the cylinders, and therefore might be shielded from the hydrodynamic interaction with the cylinders which next to the two closest cylinders. Further study is required to understand this phenomenon.

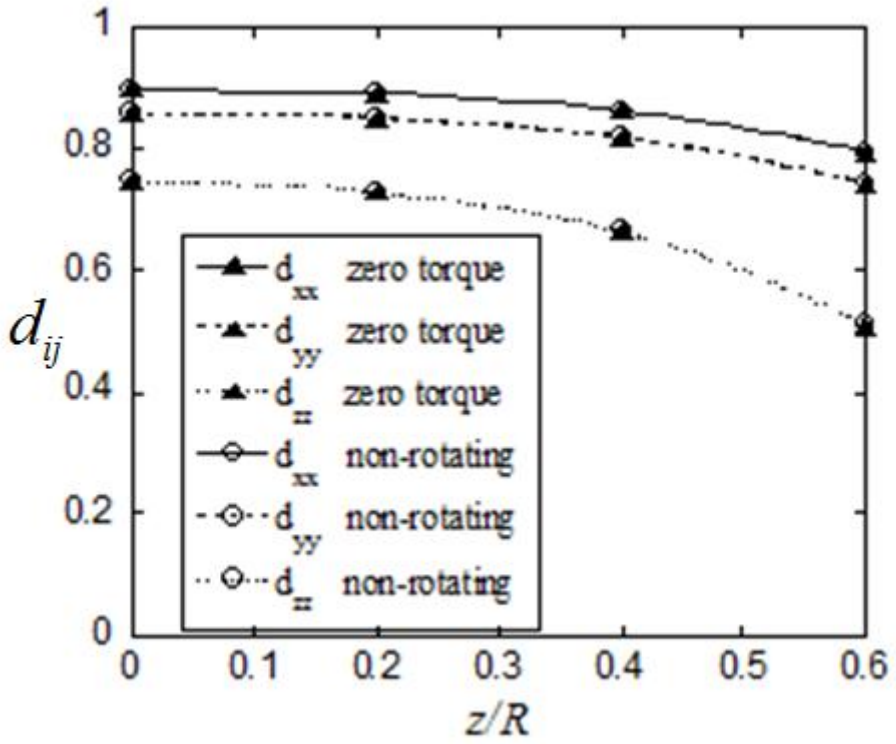

Figure 2.9 d_{xx}, d_{yy} and d_{zz} as a function of *z/R*. *L=2R*, $r_s/R = 0.2, x = 0$.

Fig. 2.9 examines the effect of the coupling between translational and rotational motion on the force coefficient tensors and the diffusive hindrance factor tensor. The diagonal components of the diffusive hindrance factor tensor is plotted as a function of *z/R*. The diffusive hindrance factor tensor obtained from Eq. 2.11 (zero torque) and that obtained from simply setting $\mathbf{f}$ equals $\mathbf{f_T}$ (non-rotating sphere) are shown to be indistinguishable graphically. In fact, neglecting the effect of rotation causes less than 1% changes in force coefficients. Also shown in Fig. 2.9 is the decrease in d_{xx}, d_{yy} and d_{zz} as a function of z. This is to be expected given that $f_{T,xx}$, $f_{T,yy}$ and $f_{T,zz}$ increases as function of z.

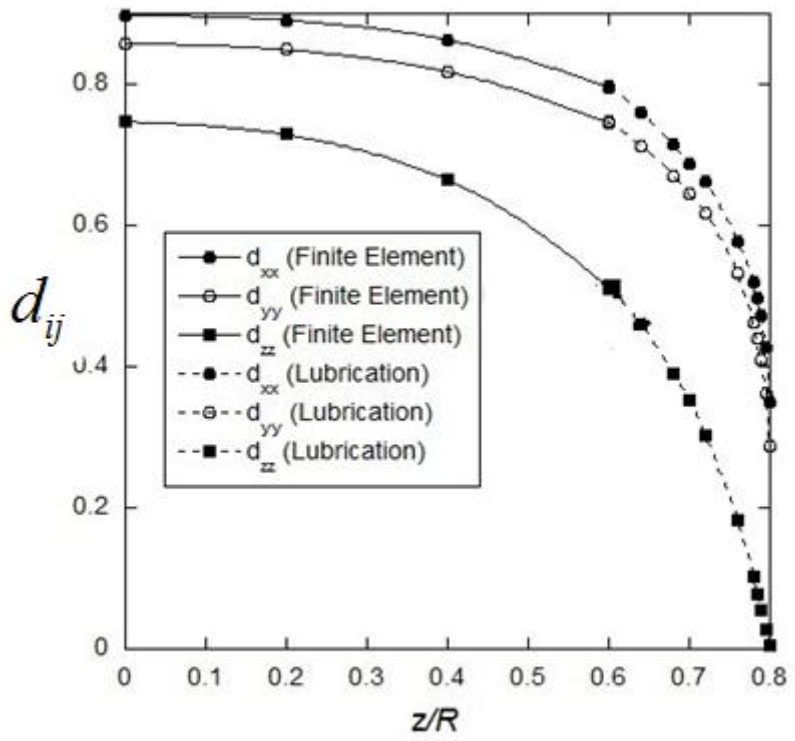

Figure 2.10 d_{xx}, d_{yy} and d_{zz} as a function of z/R for $L=2R$, $r_s/R = 0.2$ $x = 0$. Solid lines represent results obtained using finite element method. Dashed lines represent the force coefficients obtained from the lubrication expression.

Shown in Fig. 2.10 is an anisotropic nature of the diffusivity with the z-direction being the most restrictive direction at this value of x. The diagonal component of the diffusive hindrance factor tensor, **d**, is presented as a function of z/R. As show in Fig. 2.10, the diffusivity decreases until it reaches zero where the gap between sphere and cylinder and vanish at the point where the sphere touches the cylinder ($z = R+r_s$).

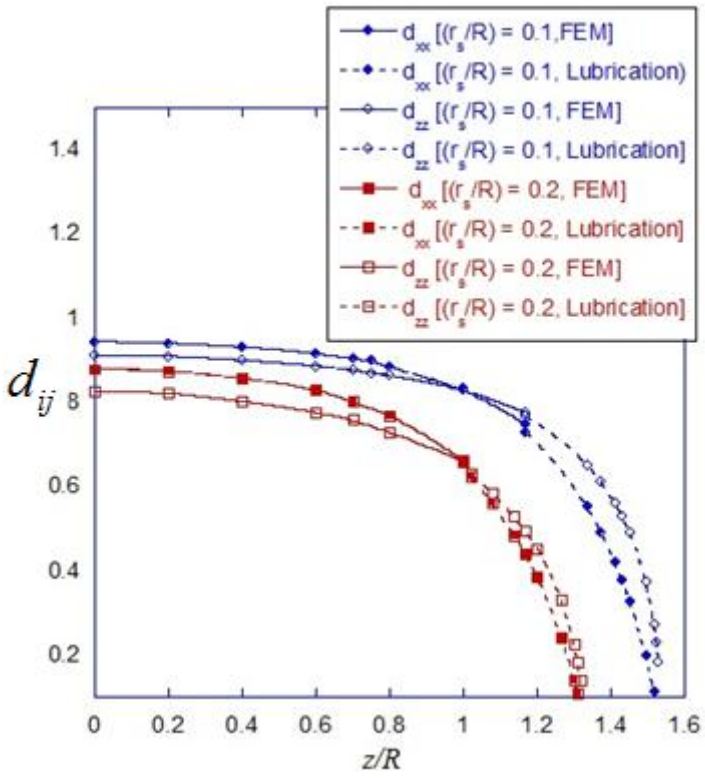

Figure 2.11 d_{xx} and d_{zz} as a function of z/R, $L=2R$, r_s/R = 0.1 and 0.2 x = -1. Dashed lines represent the force coefficients obtained from the lubrication expression.

In Fig. 2.11, d_{xx} were plotted together with d_{zz} as a function of z/R for sphere moving right below a row of cylinders (x = -1). Unlike the trend shown in Fig. 2.8, there is a cross over at z/R = 1. For z/R < 1, d_{zz} is larger than d_{xx}. However, if z/R > 1, d_{xx} is larger than d_{zz} regardless of particle sizes. This is due to the fact that, near a cylindrical fiber, a sphere moving towards a fiber will experience more drag than a sphere moving parallel to the fiber. It confirms that the particle diffusivity is anisotropic even for small particles with radii being only 10% and 20% of the distance between two adjacent cylindrical fibers.

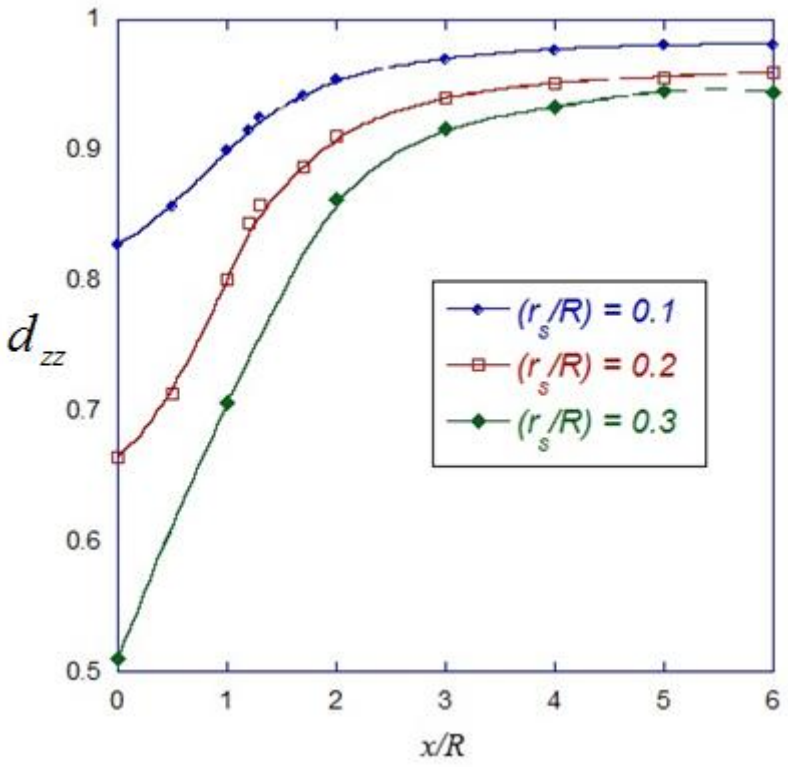

Figure 2.12 d_{zz} as a function of x/R, $L=2R$ with r_s/R = 0.1 0.2 and 0.3, z = 0.4.

In Fig. 2.12, d_{zz} is plotted as a function of x/R, the scaled distance from the row of cylinders. In keeping with the trend shown in Fig. 2.5, d_{zz} increases monotonically as x increases. Far from the cylinders, the diagonal components of the diffusive hindrance factor tensor approaches unity, verifying that the diffusivity approaches D_∞. Fig. 2.12 also demonstrates that diffusion of larger solutes experience is more restricted than that of smaller solutes.

Because of the maximum value of $f_{T,xx}$ as a function of x/R shown in Fig. 2.8, when d_{xx} is plotted as a function of x/R, there is a minimum value as shown in Fig. 2.13. Unlike the monotonic decrease of d_{zz} as a function of x, d_{xx} shows a minimum value at $x = R$ before exhibiting an increase once again. As mentioned above, this minimum point in the profile of d_{xx} was not seen in the previous work by Drumond and Deen (1995) [12], where the force coefficients were approximated using the enhanced drag on a sphere between parallel plates. As mention before, we

think that the minimum point in d_{xx} might be due to the interaction between the sphere and other cylinders apart from the two closet cylinders, but further study is still required.

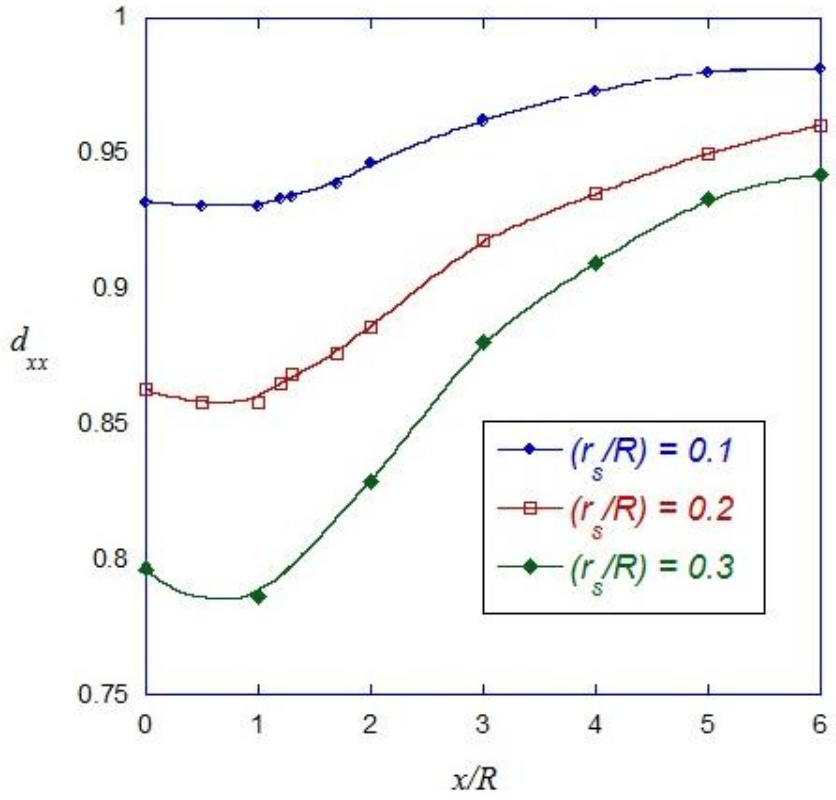

Figure 2.13 d_{xx} as a function of x/R, $L = 2R$ with r_s/R = 0.1 0.2 and 0.3, z = 0.4.

Next, we investigate the effect of the sizes of the gap between cylinders on hindered diffusion, expanding the numerical calculation to include particles with sizes comparable to the sizes of the cylinders and the gaps between them. In Fig. 2.14, d_{xx}, d_{yy} and d_{zz} are plotted as a function of particle sizes for two different gap widths, $L=2R$ and $3R$, respectively. Not surprisingly, d_{xx}, d_{yy} and d_{zz} increases as the gap width increases. d_{xx}, d_{yy} and d_{zz} decreases as the particle sizes increases, and, as always, the z-direction is the most restrictive direction for diffusion.

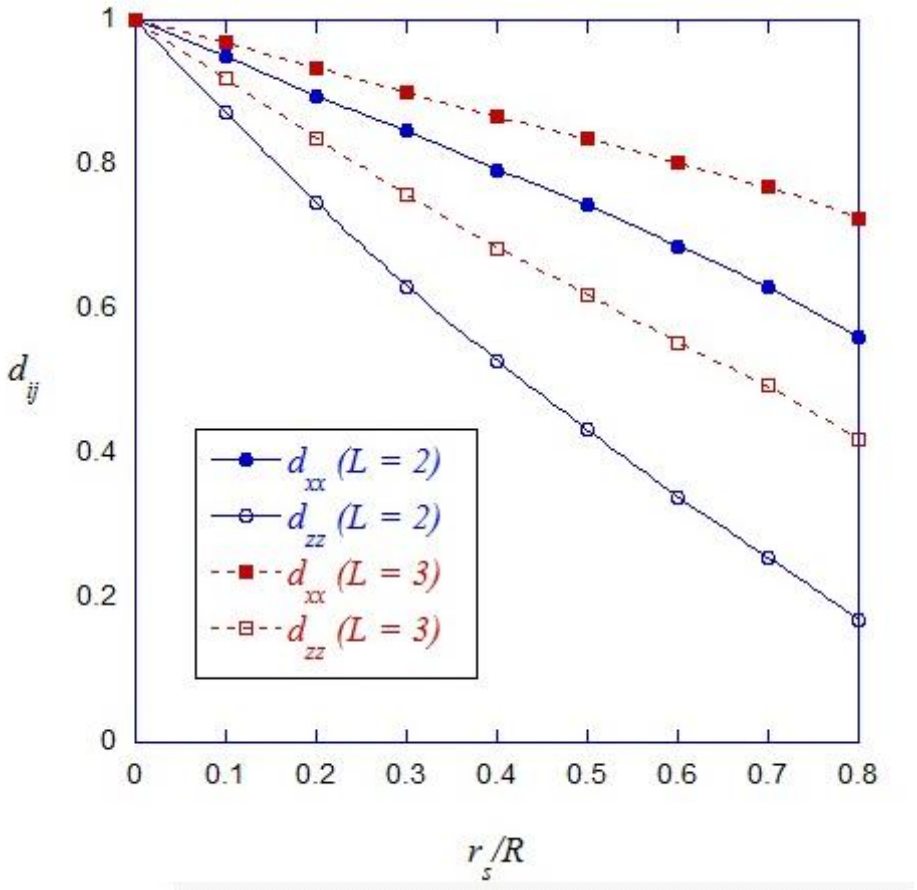

Figure 2.14. d_{xx}, d_{yy} and d_{zz} as a function of r_s/R. Results are plotted for $L = 2R$ and $3R$. Sphere is located $(x, z) = (0, 0)$.

CHAPTER III

HINDERED CONVECTION IN THE EPITHELIAL CELL LAYER AND CONVECTION-DIFFUSION EQUATION

In addition to diffusing through a slit diaphragm, the macromolecules are also convected towards the Bowman's capsule due to the pressure difference across the glomerular capillary wall. Typical value for the total filtration rate per mice glomerulus is 40 nL/min and the total glomerular filtration area is approximately 0.002 cm^2 [24]. It is generally believed that the fractional area of the epithelial slit openings (area not covered by the podocytes) is 0.11. Assuming that the fluid flux can only flow through the epithelial slit and not the podocytes, one estimates an average velocity in the epithelial slits to be $3x10^{-5}$ m/s.

This chapter is devoted to hindered convection through a slit diaphragm. There have been theoretical studies on hindered convection of a sphere in a coquette flow due to a presence of a plane wall [14], as well as hindered diffusion in cylindrical and slit pores [16], [17]. However, a study on hindered convection of a sphere passing through a row of parallel cylinders remained absent. The first section of this chapter will focus on the modification of the solute flux equation due to the non-zero upstream fluid velocity. A new force coefficient tensor due to a flow past a sphere, and a convective hindrance factor tensor will be introduced. Numerically calculated results will be presented and discussed. Finally, the convection-diffusion equation describing the transport of solute across the epithelial cell layer will be stated, and solved in order to obtain solute concentration and, ultermately, the sieving coefficient for the slit diaphragm.

3.1 Total Solute Flux through a Slit Diaphragm

As shown below, Fig. 3.1 is similar to Fig. 2.3 everywhere except for the non-zero ultrafiltration fluid velocity, $\mathbf{V}$. All assumptions employed during the calculation of the force coefficient $\mathbf{f}$ and the diffusive hindrance factor are also

assumed here. The particle is moving at a velocity **U** through a row of parallel fiber, and once again, similar to an approach used in Chapter 2 with solute velocity fluctuation neglected, the effective body force (the gradient in chemical potential) is balanced by a hydrodynamic force as shown below.

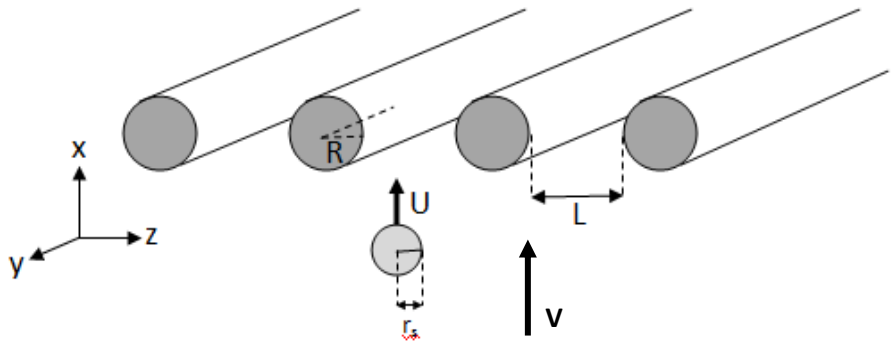

Figure 3.1 Schematic drawing for transport of spherical macromolecules through a row of infinitely long cylinders. **V** is the fluid velocity and **U** is the solute velocity.

$$-kT\nabla \ln C - 6\pi\mu r_s(\mathbf{f}\cdot\mathbf{U}-\mathbf{g}\cdot\mathbf{V}) = 0 \qquad (3.1)$$

The difference between the equation above and Eq.(2.5) is the additional term in the hydrodynamic drag due to a flow past a sphere. **g** is a second-order tensor containing force coefficients for a stationary sphere immersed in a fluid that is moving with non-zero velocity:

$$\mathbf{g} = \begin{bmatrix} g_{xx} & g_{xy} & g_{xz} \\ g_{yx} & g_{yy} & g_{yz} \\ g_{zx} & g_{zy} & g_{zz} \end{bmatrix} \qquad (3.2)$$

where the component g_{ij} is the enhance hydrodynamic drag in the i-direction acting on a stationary sphere divided by $6\pi\mu r_s V_j$ with V_j being the component in the j-direction of the local unperturbed fluid velocity (**V**) . Like **f** , values of components

of $\mathbf{g}$ depend on both particle size (r_s) and position (x and z). Combining Eqs.(2.2) and (3.1), the solute flux becomes

$$\mathbf{N} = -D_{\infty}\mathbf{d}.\nabla C + \left(\mathbf{f}^{-1}.\mathbf{g}\right)\mathbf{V}C \tag{3.3}$$

The diffusive hindrance factor tensors, $\mathbf{d}$, is defined in Eq.(2.8). The convective hindrance factor tensor, $\left(\mathbf{f}^{-1}\cdot\mathbf{g}\right)$, also a second order tensor, can be thought of as a parameter that identifies how much a convective flux is changed due to a hydrodynamic particle-fiber interaction. In absence of the row of fibers, $\left(\mathbf{f}^{-1}\cdot\mathbf{g}\right)$ is simply an identity matrix. Since $\mathbf{f}$ is already calculated and discussed extensively in Chapter 2, what remains to be determined is $\mathbf{g}$ which can be calculated from a hydrodynamic drag exerted on a stationary sphere by a passing flow.

3.2 Calculation of Force Coefficient $\mathbf{g}_{ij}$

In order to obtain g_{ij}, the velocity field and pressure is first calculated. Similarly to the methodology outlined in Chapter 2, the velocity and pressure field is calculated by solving the Stokes and continuity equation:

$$\nabla P = \mu\nabla^2\mathbf{V} \tag{3.4}$$

$$\nabla\cdot\mathbf{V} = 0 \tag{3.5}$$

Regarding the boundary conditions, the fluid velocity became a unit velocity in the z-direction far upstream and downstream as $x \to \pm\infty$. The fluid velocity profile vanishes at the particle and cylinder surfaces in order to satisfy the no-slip boundary condition. The hydrodynamic drag on the particle is obtained by integrating pressure and viscous stress all over the sphere surface.

Eqs. (3.4) and (3.5) are solved by using the commercial finite element, COMSOL Multiphysics (COMSOL, Stockholm, Sweden) operating on a 64-bits work station. Similar to $\mathbf{f}$, the effect of the coupling between translational and rotational motion on $\mathbf{g}$ is insignificant. The force coefficients calculated by having the angular velocity of the particle equals zero (non-rotating sphere) is graphically

indistinguishable to that of a sphere experiencing zero torque. The calculation is done by having the sphere not rotating.

3.3 Calculated Force Coefficient and Discussion

In order to demonstrate the effect of the sphere-cylinder hydrodynamic interaction, the numerical results will be presented as $g_{xx}V_x$ and $g_{zz}V_z$, which can be thought of as the hydrodynamic force acted on a stationary solute by a passing flow in the x and z-direction divided by the coefficient $6\pi\mu r_s$: this is shown in Eq. (3.1). If the row of cylindrical fibers is absent, $\mathbf{g}$ will simply be the identity matrix. The force on the sphere will simply be $6\pi\mu r_s\mathbf{V}$ and the convective flux will simply be the product of the solute concentration and the fluid velocity. However, because of the sphere-cylinder hydrodynamic interaction, the convective flux differs from the product of the fluid velocity and the solute concentration.

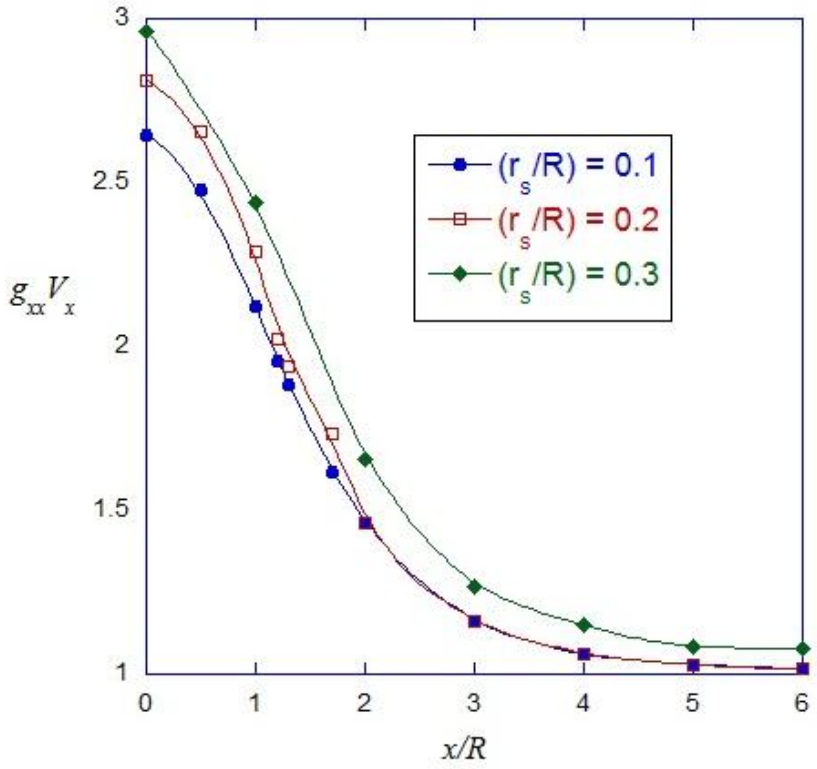

Figure 3.2 $g_{xx}V_x$, the hydrodynamic force acted on a stationary sphere by a passing flow in the x-direction divided by the drag coefficient ($6\pi\mu r_s$) as a function of x/R for z = 0.4. The results were plotted for r_s/R = 0.1, 0.2, 0.3 and $L = 2R$.

In Fig. 3.2, $g_{xx}V_x$ is plotted as a function of *x/R,* a distance between the sphere and the row of fibers. The sphere located at x = 0 would mean that the sphere is located in the closest gap between two adjacent fibers (right in the row of fibers). The hydrodynamic force on a stationary sphere in the x-direction monotonically increases when the sphere approaches a row of fibers (or, in other words, as *x* approaches zero) and decreases until it reaches 1 as the distance between the sphere and the row of fiber increases. Increasing the solute size seems to enhance the force in this direction. $g_{xx}V_x$ for r_s/R = 0.3 is larger than that of r_s/R = 0.1 and 0.2.

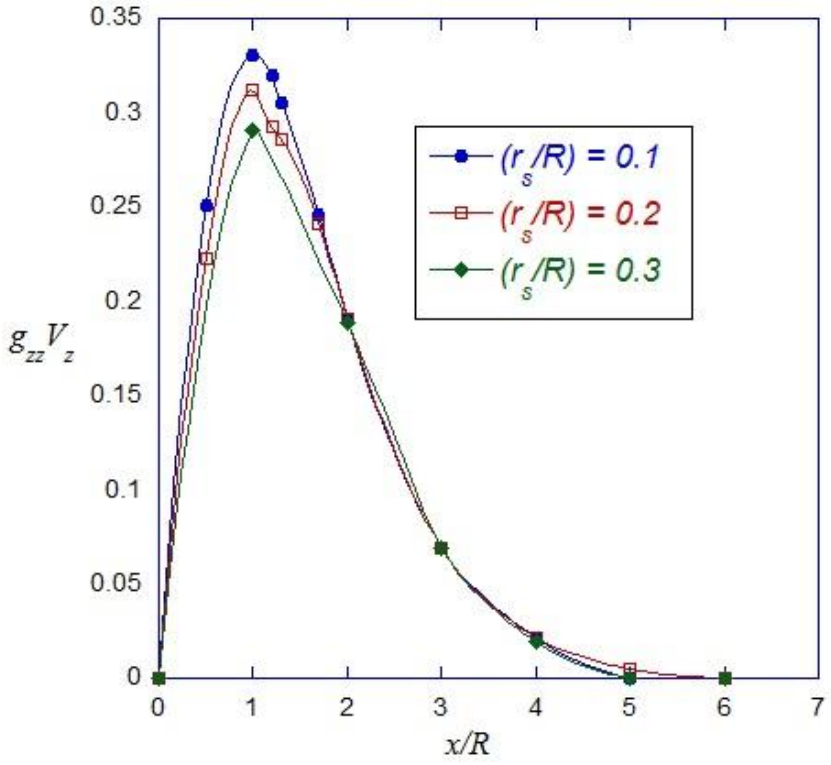

Figure 3.3 $g_{zz}V_z$ the hydrodynamic force acted on a stationary sphere by a passing flow in the z-direction divided by the drag coefficient ($6\pi\mu r_s$) as a function of *x/R* for z = 0.4. The results were plotted for r_s/R = 0.1, 0.2, 0.3 and *L = 2R*.

$g_{zz}V_z$ is shown in Fig 3.3 as a function of *x/R*. Unlike the trend of $g_{zz}V_z$ shown in Fig. 3.2, the hydrodynamic force imposed on a stationary sphere by a passing flow in the z-direction first increases as a function of x until it reaches a maximum point at *x/R* = 1, then decreases and dies out as the distance between the sphere and the row of cylinders increases. This is due to the fact that, far from the row of cylinders, the fluid velocity in the z-direction equals zero. Also unlike $g_{xx}V_x$, an increase in solute size decrease the hydrodynamic force on the sphere in the z-direction: $g_{zz}V_z$ for r_s/R = 0.3 is lower than that of r_s/R = 0.1 and 0.2.

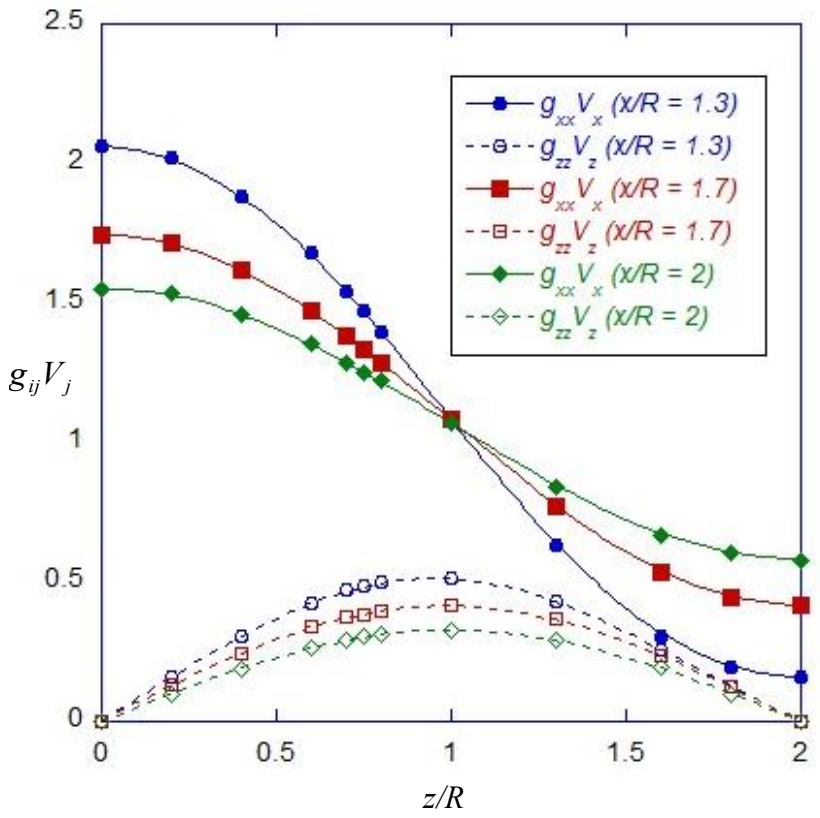

Figure 3.4 $g_{xx}V_x$ and $g_{zz}V_z$, the hydrodynamic force on a stationary sphere in the x and z-direction divided by the drag coefficient ($6\pi\mu r_s$) as a function of *z/R*. The solid line are the convective flux in the x-direction and the dashed line are the convective flux in the z-direction The results were plotted for three value of *x/R* for *L = 2R*.

In Fig. 3.4, $g_{xx}V_x$ and $g_{zz}V_z$ are plotted as a function of *z/R* for three values of *x/R* (three different values of distance between the sphere and the row of cylinders). Note that having a sphere located at z = 0 means that it is located with equal distances from two adjacent fibers (shown below in Fig. 3.6). $g_{xx}V_x$, the hydrodynamic force on a stationary sphere in the x-direction, decreases as z/R increases: this is to be expected since the fluid velocity in the x-direction is maximum at z = 0 (farthest distance from the cylinders at a given value of x) and vanishes at the cylinder surfaces due to the

no-slip boundary condition. On the other hand, $g_{zz}V_z$, the hydrodynamic force on a stationary sphere in the z-direction, first increases until it reaches a maximum point at z/R = 1 and then decreases: a trend also shared with fluid velocity in the z-direction. It can be seen that the magnitude of $g_{xx}V_x$ is always larger than the magnitude of $g_{zz}V_z$ because the fluid velocity in the x-direction is larger than the fluid velocity in the z-direction.

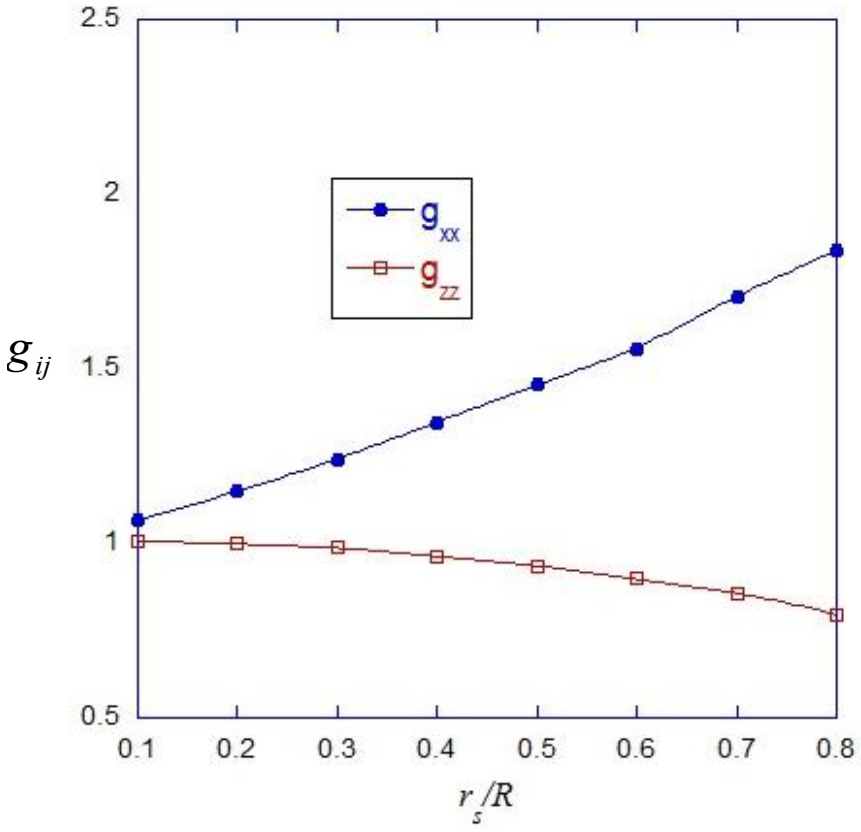

Figure 3.5 g_{xx} and g_{zz} as a function of r_s/R. Results are plotted for $L = 2R$. Sphere locate at x = -2 and z = 1.

Next, we investigate the effect of hydrodynamic interaction from the flow on sphere with various particle sizes, expanding the numerical calculation to include particles with sizes comparable to the sizes of the cylinders. In Fig. 3.5, g_{xx} and g_{zz}

are plotted as a function of particle sizes. The enhanced hydrodynamic drag in the x-direction, g_{xx}, increases as the particle sizes increase. On the other hand, the enhanced hydrodynamic drag in the z-direction, g_{zz}, decreases as a function of solute sizes. Having the stationary sphere immersed in the flow and blocking the flow forces the fluid to move more along the x-direction, and hence the increase of g_{xx} and the decrease of g_{zz} as a function of particle sizes.

After the calculation of the hindered transport parameters, $\mathbf{f}$, $\mathbf{d}$ and $\mathbf{g}$, is completed, we proceed to calculate the solute concentration across the slit diaphragm.

3.4 Convection-Diffusion Equation

Fig. 3.6 is a schematic drawing of a region where, in order to determine a solute concentration across a slit diaphragm, the solute conservation equation, stated below, must be solved.

$$\frac{\partial C}{\partial t} = -\nabla \cdot \mathbf{N} \tag{3.6}$$

Pseudo-steady state is assumed since the time scale of the change in blood pressure is much larger than the time scale of solute diffusion and convection across the slit diaphragm. Substituting the flux expression from Eq. (3.3) and rewriting Eq. (3.6) in a semi-dimensionless form, we have

$$\widetilde{\nabla}.(-\mathbf{d}.\widetilde{\nabla}C + Pe\mathbf{d}\cdot\mathbf{g}\cdot C\widetilde{\mathbf{V}}) = 0 \tag{3.7}$$

where $\widetilde{\nabla} = R\nabla$ with R being the radii of cylindrical fibers. $\widetilde{\mathbf{V}} = \mathbf{V}/V$ where V is the undisturbed fluid speed far from the row of fiber. Pe is the Peclet number: a ratio between convection and diffusion time scale of fluid transport defined as

$$Pe = \frac{VR}{D_\alpha} \tag{3.8}$$

If Pe >>1, convection dominates the transport process. On the other hand, if Pe <<1, diffusion will be relatively more important. Typically reported values for R is about 2-10 nm, with the solute diffusivity (at 37ºC) being about 10^{-11}-10^{-10} m^2/s, Pe is approximately 10^{-5}-0.1 which means that diffusion is a more dominant process.

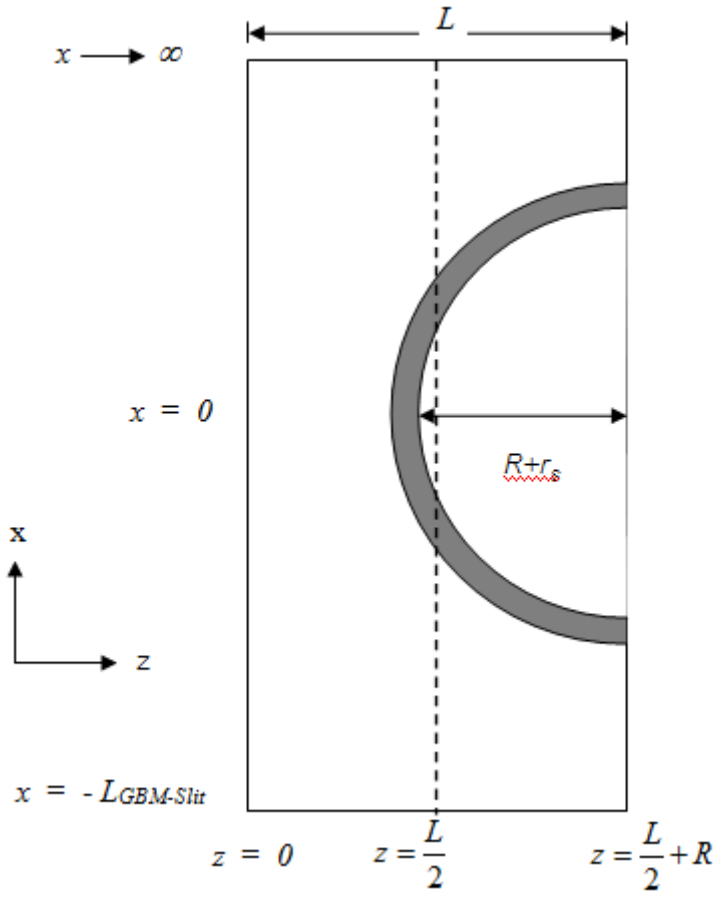

Figure 3.6 Division of the computational domain. The domain was one-half of the space between two adjacent cylinders. The GBM-epithelial slit interface is assumed to be at $x = -L_{\text{GBM-Slit}}$. R and r_s are the cylinder radius and sphere radius, respectively. Lubication theory is employed in the shaded area.

The hindrance factor tensors, $\mathbf{d}$ and $\mathbf{g}$, are defined in Eqs.(2.8) and (3.2), respectively. As shown in Fig. 3.6, the region, where Eq.(3.7) is to be solved, is

divided into 2 regions. In Region I, the force coefficients are computed using COMSOL Multiphysics. In Region II, the hindrance factor tensors are calculated from hydrodynamic drag obtained by Falade and Brenner [23].

In order to determine the solute concentration, Eq. (3.7) is solved with the following boundary conditions:

$$N_x = N_0 \qquad \text{at} \qquad x = -L_{\text{GBM-Slit}} \tag{3.9a}$$

$$C = C_B = \frac{N_0}{V} \qquad \text{at} \qquad x \to \infty \tag{3.9b}$$

$$N_z = 0 \qquad \text{at} \qquad z = 0\,,\ z = \frac{L}{2} + 1 \tag{3.9c}$$

$$N_r = 0 \qquad \text{at} \qquad r \equiv (x^2 + z^2)^{\frac{1}{2}} = R + r_s \tag{3.9d}$$

Eq.(3.9a) states that the upstream solute flux at a distance $x = -L_{\text{GBM-Slit}}$ from the center of the cylinders is constant, which is the flux flowing from the GBM into the epithelial slit (N_0). As shown in Eq. (3.9b), far downstream from the row of fibers, the concentration reaches a constant which is a solute concentration in Bowman's capsule (C_B). Eq.(3.9c) expresses symmetry at $z = 0$ and $z = \frac{L}{2} + 1$ due to the fact that the slit diaphragm is assumed to be a row of infinite number of parallel cylinders. Stated in Eq.(3..9d) is the boundary condition stemmed from the sphere-cylinder steric interaction; the distance between the center of the sphere and the cylinder cannot be less than the sphere radius (r_s). The solute flux normal to the cylinders must vanish at the distance r_s from the cylinder surfaces because of the no-penetration condition: the solutes cannot penetrate into the cylindrical fibers.

In order to solve Eq. (3.7) along with boundary conditions stated in Eqs.(3.9a)-(3.9d), the dimensionless fluid velocity or $\tilde{\mathbf{V}}$ must be specified at every

location. To that purpose, the Stokes and continuity equation (Eqs.(2.13) and (2.14)) are solved by using COMSOL Multiphysics with the following boundary conditions:

$$V_x = V \ , V_z = 0 \qquad x = -L_{\text{GBM-Slit}} \ \text{and} \ \ x \to \infty \quad \text{(3.10a)}$$

$$V_z = 0 \qquad \text{at} \qquad z = 0 \ , z = \frac{L}{2} + 1 \quad \text{(3.10b)}$$

$$V = 0 \qquad \text{at} \qquad r \equiv (x^2 + z^2)^{\frac{1}{2}} = R + r_s \quad \text{(3.10c)}$$

The fluid velocity became a constant velocity in the x-direction far upstream and downstream as $x \to \pm\infty$ as stated in Eq.(3.10a). Eq.(3.10b) expresses symmetry at $z = 0$ and $z = \frac{L}{2} + 1$ Eq.(3.10c) is simply the no-slip boundary condition at the particle and cylinder surfaces.

After obtaining the fluid velocity, Eq. (3.7), with boundary conditions shown in Eqs. (3.9a)-(3.9d) are solved by using the commercial finite element, COMSOL Multiphysics (COMSOL, Stockholm, Sweden) operating on a 64-bits work station.

3.5 Sieving Coefficient of the Slit Diaphragm

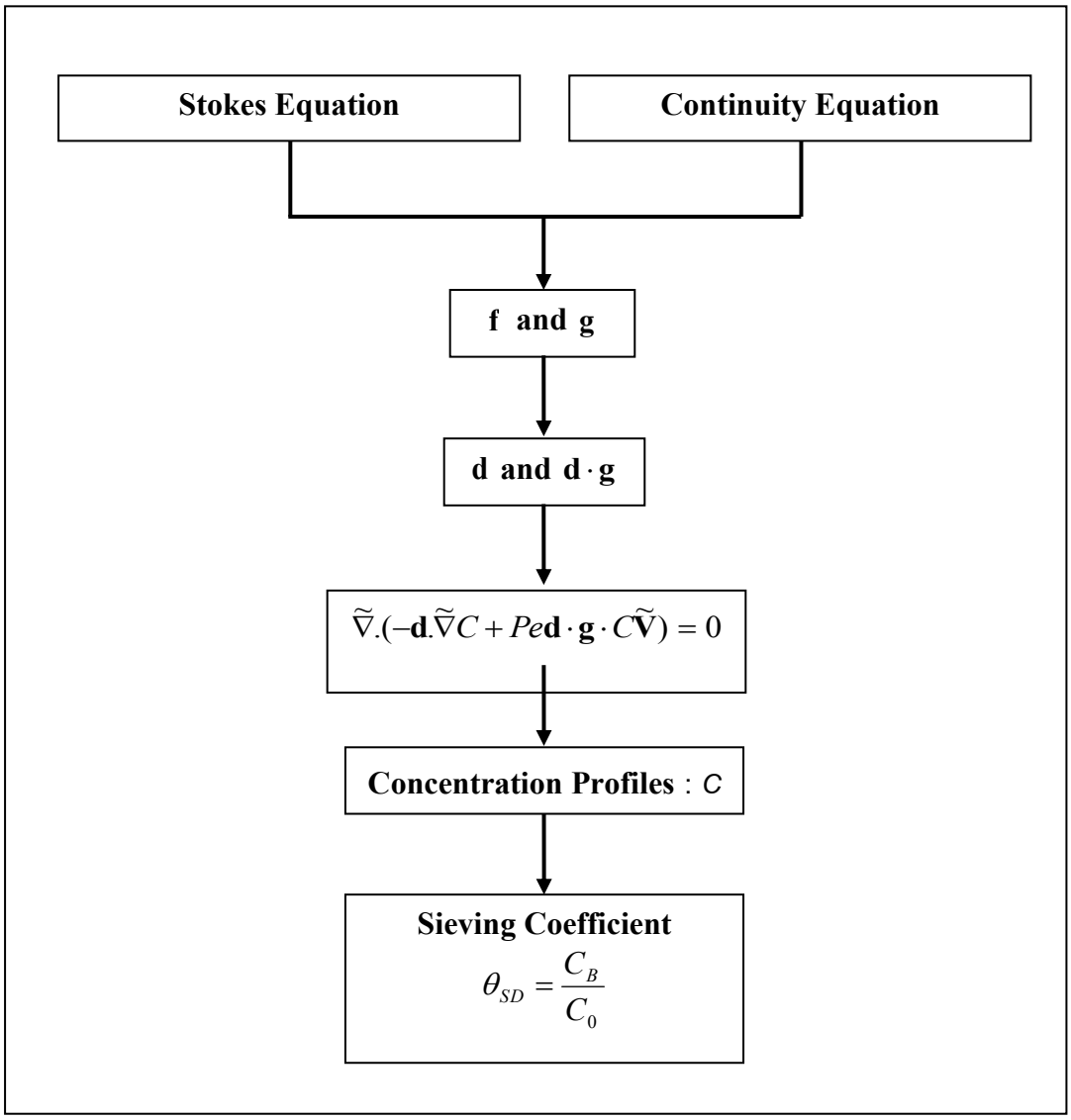

Figure 3.7 Procedure of calculation of sieving coefficient for the slit diaphragm.

Fig. 3.7 demonstrates the calculation procedure of the solute concentration and the sieving coefficient through the slit diaphragm. First, Stokes' equation and the continuity equation are solved in order to obtain the force coefficient tensors: $\mathbf{f}$ and $\mathbf{g}$. Then $\mathbf{f}$ and $\mathbf{g}$ are converted to the hindrance factor tensors : $\mathbf{d}$ and $\mathbf{d}\cdot\mathbf{g}$. In order to determine the solute concentration, the convection diffusion equation is solved. Finally, the sieving coefficient of slit diaphragm is calculated as a ratio between solute concentration down-stream in Bowman' space (C_B) and solute concentration up-stream from GBM-epithelial interface (C_0).

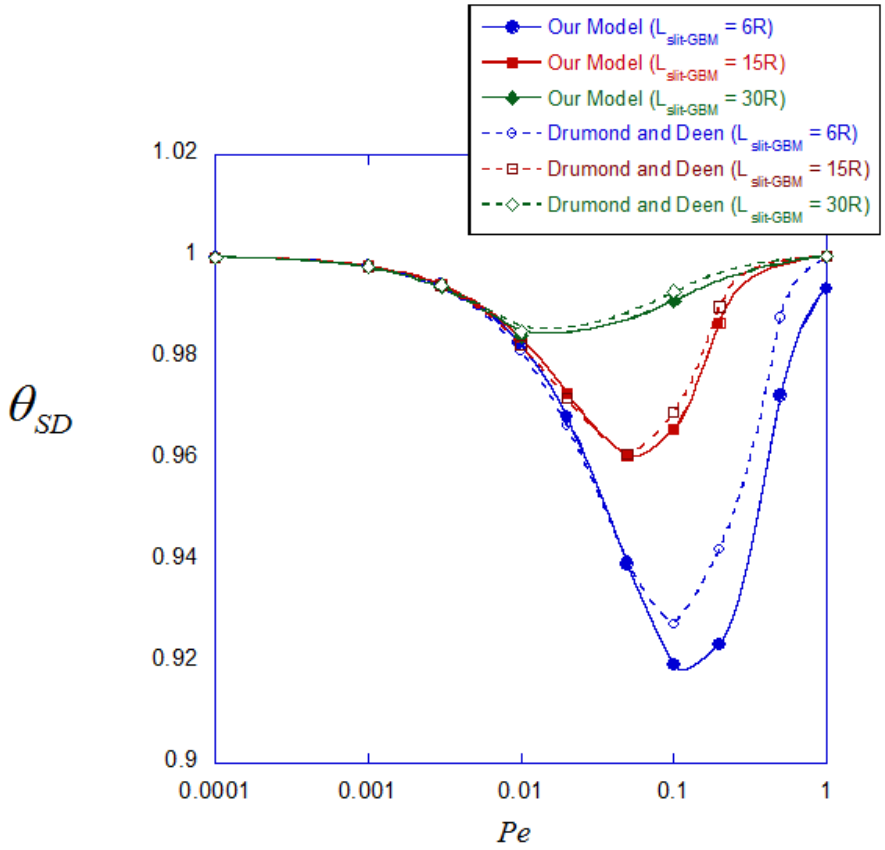

Figure 3.8 Sieving coefficient of slit diaphragm, θ_{SD} as a function of Peclet number. Our results (solid lines) are compared with previous work by Drumond and Deen (dashed lines) [12]. $L_{\text{GBM-Slit}} = 6R$, $15R$ and $30R$, $r_s/R = 0.2$ and $L = 2R$.

Fig. 3.8 shows the effect of Pe on θ_{SD}. Recall that Pe is a ratio between convection and diffusion time scale of fluid transport which defined in Eq.(3.8). For $Pe \to 0$, there is diffusional equilibration across the slit diaphragm. The upstream and downstream concentration are equal and $\theta_{SD} \to 1$. As Pe increase, θ_{SD} at first decreases and then eventually returns to unity. An increase in Pe creates 2 factors. First, it creates a concentration drop near the row of cylinder; the larger the Peclet number is, the larger the concentration drop becomes. This effect enhances the sieving coefficient. Second, it causes the concentration polarization upstream from the

cylinders; the solute are accumulated at x<0. This is shown as a peak in Fig.3.9; the maximum concentration increases with increasing Pe . This causes a decline in θ_{SD}.

The minimum values of θ_{SD} is based on $L_{\text{GBM-Slit}}$ (the distance between GBM and slit diaphragm). As $L_{\text{GBM-Slit}}$ increases, the minimum value of θ_{SD} becomes closer to unity. In Fig. 3.8, our results show the same trend as that of Drumond and Deen [12], although our value of θ_{SD} is slightly lower. When the curvature effect are take into account, θ_{SD} seem to be lower: an effect we think might be even more significant for larger macromolecules. In the next chapter, the calculation of solute concentration across the GBM and the overall glomerular sieving coefficient will be described.

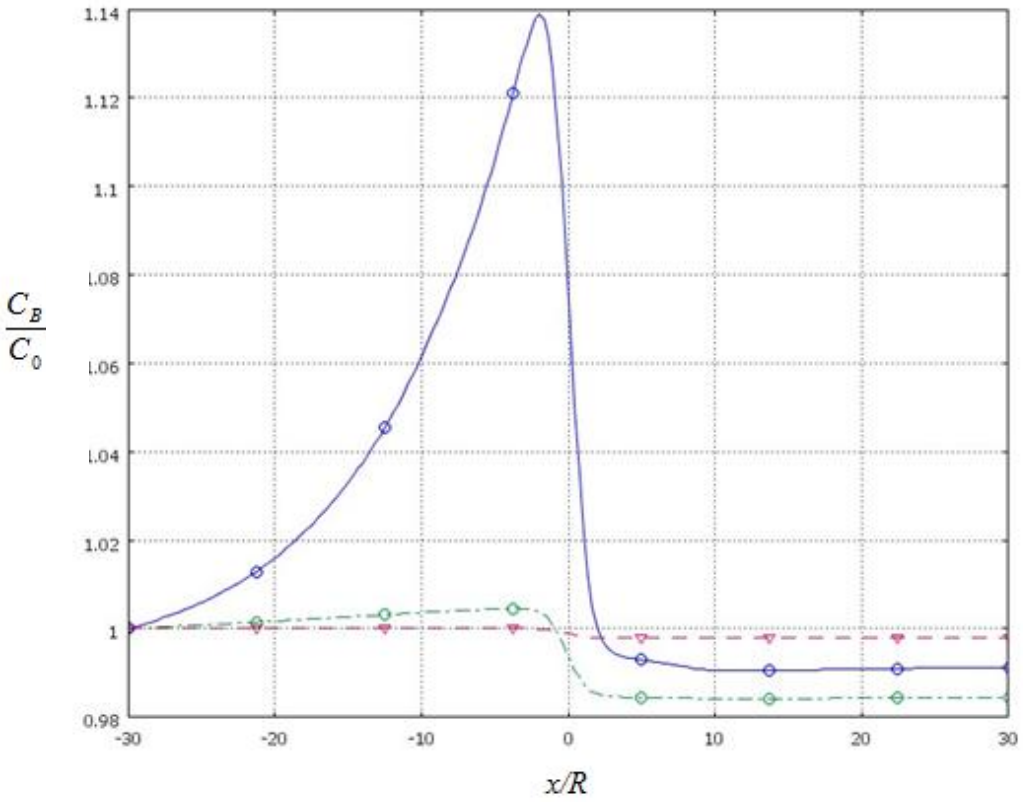

Figure 3.9 $\frac{C_B}{C_0}$ as a function of *x/R*. Results are plot for three values of Pe : Pe =0.1 (blue line), Pe = 0.01 (green line) and Pe = 0.001 (red line) with $L_{\text{GBM-Slit}}$ =30.

CHAPTER IV

OVERALL GLOMERULAR SIEVING COEFFICIENT

As mentioned in Chapter 1, we want to relate the overall glomerular sieving coefficient of electrically-neutral solutes to nanostructures of the GBM and the epithelial slit. As shown in Eq.(1.3), the overall sieving coefficient (θ) of such molecules is simply the product of solute sieving coefficient for the GBM (θ_{bm}) and the slit diaphragm (θ_{SD}). Details of calculation of sieving coefficient for the slit diaphragm are given in Chapter 3. This chapter will therefore begin with the mathematical model developed to explain transport of macromolecules through GBM, followed by an overview of existing experimental results of sieving coefficient of neutral or slightly cationic myoglobin as well as that of ficoll, a spherical highly-crosslinked poly-saccharide. A comparison between our calculated overall sieving coefficient and data from experiment employing the tissue-uptake technique will be made.

4.1 Transport of Solutes across Glomerular Basement Membrane (GBM)

4.1.1 Isolated GBM

GBM is generally considered to be a hydrogel consisting of approximately 90% water and 10-11% fibers. The fibers are collagen type IV (fiber radii=$r_f = 3.5\,\text{nm}$), proteoglycan with a protein core and glycoaminoglycan (GAG) chain ($r_f = 0.5\,\text{nm}$) as well as other fibers such as laminin etc. This section aims to create a mathematical model capable of explaining the transport of spherical solutes through GBM.

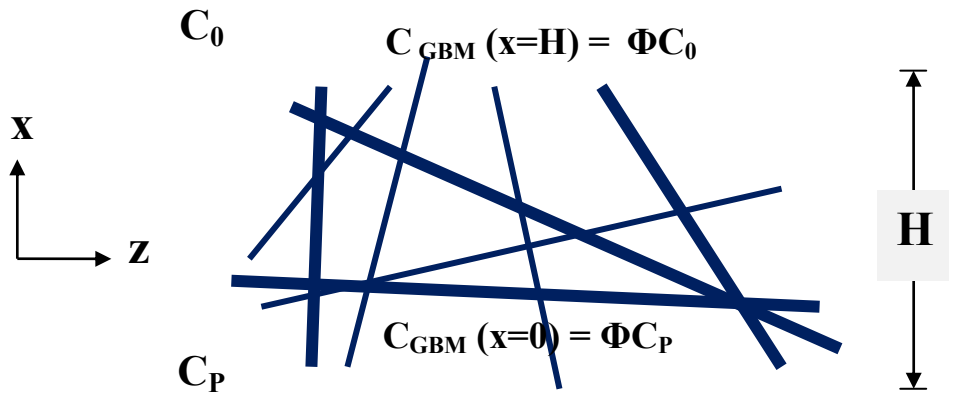

Figure 4.1 Two-dimensional approximation of ultrafiltration of macromolecule through an isolated GBM. C_P = the upstream macromolecule concentration in the blood stream. C_0 = the solute concentration at the GBM-epithelium interface. Upstream pressure is larger than downstream pressure, creating a flow in the x-direction.

An isolated GBM is modeled as an isotropic medium as depicted in Fig. 4.1. Solute concentration can be obtained by solving a convection and diffusion equation:

$$\frac{\partial C}{\partial t} = K_d D_\infty \frac{\partial^2 C}{\partial x^2} - K_c V' \frac{\partial C}{\partial x} \qquad (4.1)$$

where C is the macromolecule concentration and V' is the fluid velocity. D_∞ is the macromolecule diffusivity in an unbounded fluid. Note that, because the hydrogel is assumed to be isotropic, the convection-diffusion equation has become one-dimensional. Because of the hydrodynamic and steric interaction between the macromolecule and the fibers in the hydrogel, the sphere diffusivity inside the GBM will be less than D_∞: a fact characterized by the diffusive hindrance factor (K_d). In addition, its convective flux is also altered, and that is represented by the convective hindrance factor (K_c). As shown in Fig. 4.1, the macromolecule concentration has to satisfy the following boundary conditions:

$$C(x=0) = \Phi C_p \qquad (4.2a)$$

$$C(x=H) = \Phi C_0 \qquad (4.2b)$$

where the equilibrium partition coefficient (Φ) is the ratio between the solute concentration right inside and right outside the hydrogel. ϕ is a fiber volume fraction and r_s is the Stokes-Einstein radius of the molecule. Assuming that K_d and K_c are constant, steady state solution of Eq. (4.1) results in the sieving coefficient of macromolecules through GBM being

$$\theta_{\mathrm{bm}} = \frac{C_0}{C_p} = \frac{\Phi K_c}{\theta_{SD}(1-\exp(-Pe')) + \Phi K_c \exp(-Pe')} \tag{4.3}$$

where the Peclet number (Pe') is the ratio between the time scale of diffusion and the time scale of convection across the GBM defined as follows.

$$Pe' = \frac{K_c V' H}{K_d D_\infty} \quad . \tag{4.4}$$

H is the thickness of the GBM. From Eq.(4.4), one can see that the sieving coefficient for GBM also depends on the sieving coefficient for the slit diaphragm. Once the values of, θ_{bm}, Φ, K_d and K_c are known, the sieving coefficient (θ_{bm}) can be readily calculated.

1. Transport parameter calculation

(1) The equilibrium partition coefficient (Φ), defined as the ratio between the solute concentration right inside the hydrogel and the solute concentration right outside the hydrogel, is calculated using the Ogston's equation:

$$\Phi = \exp\left[-\phi\left(1+\frac{r_s}{r_f}\right)^2\right] \tag{4.5}$$

(2) Diffusive hindrance factor (K_d) can be thought of as the ratio between the solute diffusivity inside the GBM and that of a solute in an unbounded fluid. As mentioned before, GBM is a hydrogel consisting mainly of two different-sized fibers, but a calculation of hydrodynamic drag or diffusive hindrance factor of a sphere moving in a fibrous media with two different-sized randomly-oriented fibers

has not been done. There exist, however, two different approaches that can be used to calculate K_d as follows:

a) Brinkman's medium approach, often employed for calculation of hindered transport parameter in porous medium with unknown nanostructure and known hydraulic permeability. The fluid velocity and pressure inside the medium is described by Brinkman's equation:

$$-\nabla P + \mu \nabla^2 \mathbf{V} - \frac{\mu}{\kappa}\mathbf{V} = \mathbf{0} \qquad (4.6)$$

where κ is the Darcy's permeability. Brinkman's equation is essentially the extension of Darcy's equation where the fluid velocity is described as linearly proportional to the pressure difference and inversely proportional to the viscosity (μ):

$$\mathbf{V} = -\frac{\kappa}{\mu}\Delta P \qquad (4.7)$$

The effect of the nanostructure of the medium on fluid transport is described by κ, the Darcy's permeability. The second term on the right in Brinkman's equation (Eq. (4.6)) is simply the added viscous dissipation term. The experimentally measured value for κ from an isolated GBM is 2-3 nm^2. The hydrodynamic drag on a sphere moving in a Brinkman's medium is calculated by Anderson and Solomentev [20] and the diffusive hindrance factor is given in the following equation:

$$K_d = \left(1 + \frac{r_s}{\sqrt{\kappa}} + \frac{1}{9}\left[\frac{r_s}{\kappa}\right]^2\right)^{-1} \qquad (4.8)$$

b) the assumption that GBM is a hydrogel with randomly-oriented cylindrical fibers of uniform sizes. The expression for K_d for spherical solute moving in a liquid-filled fibrous media consisting of fibers of uniform sizes was developed by Claque and Phillips(1996) as shown below.

$$K_d = e^{-a\phi^b} \qquad (4.9)$$

where

$$a = 3.727 - 2.460\frac{r_f}{r_s} + 0.822\left(\frac{r_f}{r_s}\right)^2 \qquad (4.10a)$$

$$b = 0.358 + 0.366\frac{r_f}{r_s} - 0.0939\left(\frac{r_f}{r_s}\right)^2 \qquad (4.10b)$$

(3) Convective hindrance factor (K_c) is a parameter that determined how the convective flux is changed due to the presence of the fibers. There has not been a analytical or numerical of calculation of K_c of a sphere moving in fibrous media. Phillips et al. [18] suggested a calculation of K_c using the following equation:

$$K_c = \frac{1}{1-\phi} \qquad (4.11)$$

where ϕ is fiber volume fraction.

2. GBM fiber radii

It is clear from the above equations that, in order to calculate the transport parameters of the GBM, the fiber radii must be determined. As mentioned before, the fibers within GBM are mainly type IV collagens with diameter of 7 nm (r_f = 3.5 nm) and GAG chains with diameter of 1 nm (r_f = 0.5 nm). The overall volume fraction of the fibers is believed to be 10-11 % but the exact volume fractions of each type of fibers are not known. Amsden [30] has developed an expression for Darcy's permeability of a hydrogel consisting of randomly-oriented cylindrical fibers as follows:

$$\kappa = 0.31 r_f^2 \phi^{-1.17}. \qquad (4.12)$$

The value reported for κ of the GBM is 2.7 nm^2, and if the volume fraction is assumed to be 0.1, then the fiber diameter is roughly 1.6 nm (r_f is approximately 0.81 nm).

3. Sieving coefficient for an isolated GBM

Table 4.1 Parameter values for transport of macromolecules across GBM.

Parameter	Values
The width of GBM (W_{BM})	360 nm
The thickness of GBM (L)	200 - 400 nm
The volume fraction of solid in GBM (ϕ)	0.111
The fractional area of GBM covered by the slits opening (ε_s)	0.11
The fractional area of GBM covered by the fenestrae opening (ε_f)	0.2

Shown in Fig. 4.2 is θ_{bm} calculated as a function of solute sizes [24], and compared to sieving coefficient obtained from an ultrafiltration through an isolated rat GBM performed by Bolton et al. [25]. As shown in Fig. 4.3, the numerical procedures are performed with three values of fiber radii : r_f = 0.5 nm (blue lines) which is the fiber radii of the GAG chain, r_f = 0.81 nm (red lines) obtained from the experimentally measured Darcy's permeability, and r_f = 3.5 nm (green lines) which is the fiber radii of type IV collagen.

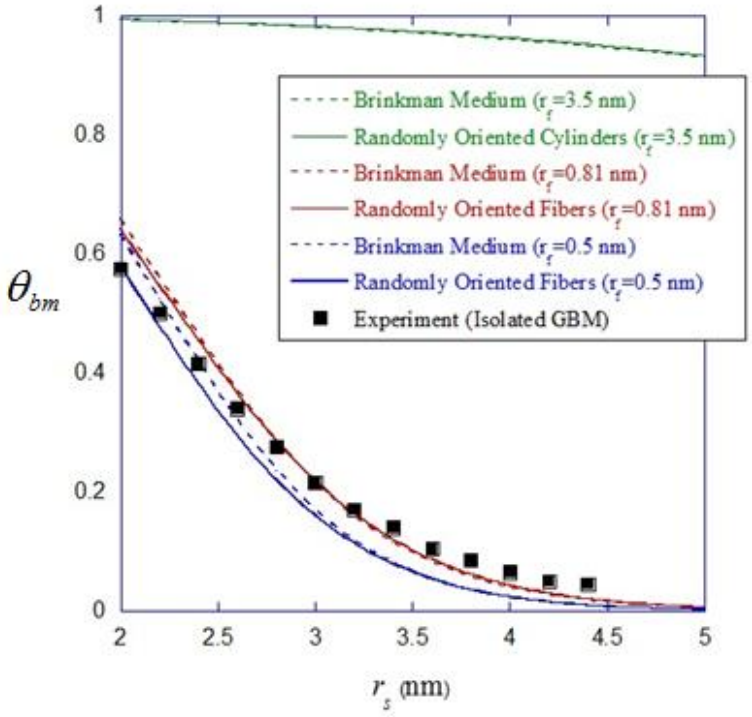

Figure 4.2 Sieving coefficient through GBM (θ_{bm}) as a function of Stokes-Einstien radius of the macromolecule (r_s) [24]. Also shown are the experimental results of ficoll filtrated through an isolated GBM [25].

As shown in Fig. 4.2, having the fiber radii being 3.5 nm greatly overestimates the sieving coefficient. Mathematical models with fiber radii equal to 0.5 nm and 0.81 nm yield sieving coefficient that is closer to the experimental data of ficoll.

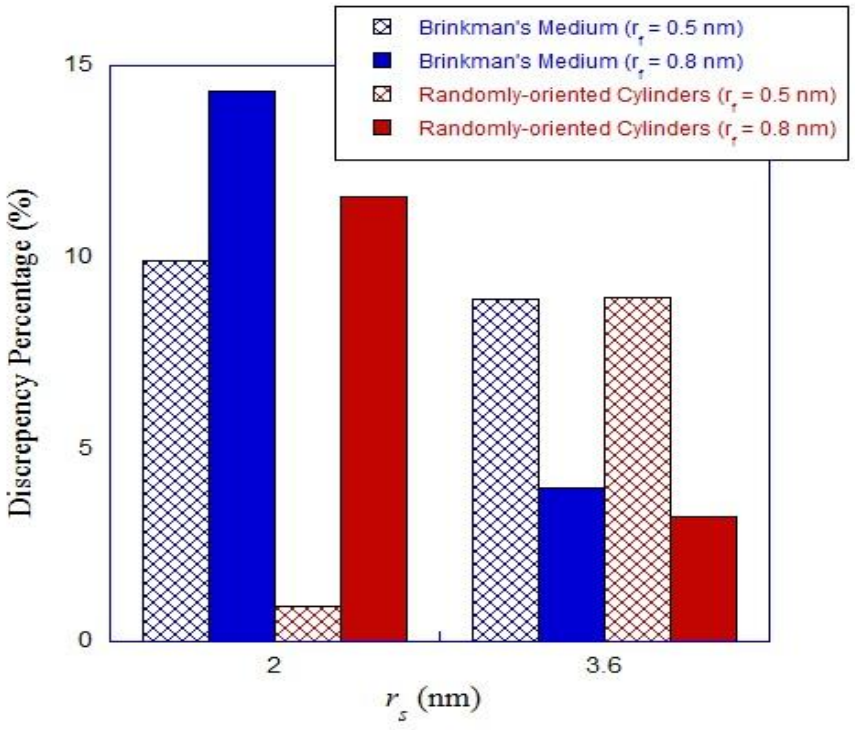

Figure 4.3 Percentage of discrepancy between numerically calculated sieving coefficient for the GBM and the experimental data [25] with r_s = 2 nm (myoglobin) and 3.6 nm (BSA).

Fig 4.3 presents the percentage of the discrepancy between the numerical calculation and the experimental data [24] at two particular solute radii: 2 nm (radii of myoglobin) and 3.6 nm (radii of bovine serum albumin (BSA), another bio-marker). At lower values of r_s, the value of fiber radii that yields the closest value to the experimental data is 0.5 nm, while at higher values of r_s, having fiber radii being 0.81 nm gives a lower percentage of discrepancy.

4.1.2 Cellular Blockage

As shown in Fig. 1.4, parts of the GBM surfaces are covered by cellular layers, and that alters the flow as well as the solute flux. It is typically believed that the fractional area of endothelial fenestrae (ε_f : GBM surface area not covered by endothelial cells) is about 0.2, and the fractional area of the epithelial slit (ε_s: GBM surface area not covered by podocytes) is approximately 0.11. With the structural unit shown in Fig. 4.1 as a framework along with a comparison between experimental data on the transport of Ficoll in isolated GBM and intact glomerular capillaries, Edwards et al. (1997) developed a model for the filtration of uncharged macromolecules in vivo [29]. The concentration field within the GBM was computed by solving Eq. (4.5) with appropriate boundary conditions that include the cellular blockage of the solute fluxes at either ends. It was found that the in-vivo sieving coefficient of the GBM could be found by replacing *Pe′* in Eq. (4.7) with *Pe** defined below.

$$\frac{Pe^*}{Pe'} = 1 + A\left(1 - \varepsilon_s \varepsilon_f\right)^B \left(\frac{H}{W}\right)^D \tag{4.13}$$

where A = 0.7366, B = 11.9864 and D = 1.2967. With the physiological parameters mentioned in this section as well as in the introduction of this chapter, *Pe** is roughly *2Pe′*. In other words, having the cellular blockage increases the Peclet number in GBM by two folds, which may partially be explained by the increase in path length of macromolecules in GBM due to the diverging-converging flow.

4.2 Overview of Existing Experimental Data

As mentioned in Chapter 1, we are particularly interested in the transport of myoglobin, a bio-marker of muscle damage and one of the causes of acute renal failure. There has been several experiments done in order to determine the glomerular sieving coefficient of myoglobin. A technique usually employed is the tissue uptake of radiolabled tracers administered in vivo. Radioactivity is counted in plasma, urine and the removed kidneys, allowing for a calculation of sieving coefficient [1]. For

nMyoglobin, an electrically-neutral myoglobin with radius of 1.96 nm, the reported value of its sieving coefficient in rats is 0.77 [26]. In the case of cMyoglobin, a slightly cationic myoglobin with radius of 17.5 nm, its reported sieving coefficient is slightly lower at 0.74 [27]. The sieving coefficient of ficoll, highly-crosslinked electrically-neutral spherical polysaccharide molecules with radius being 2 nm (close to radii of myoglobins), obtained by the tissue-uptake technique, is 0.7-0.8 [28].

4.3 Calculation of Glomerular Sieving Coefficient of Myoglobin

To establish an approximate range for R (fiber radius of the slit diaphragm), we used reported sizes based on the electron micrographs of glomerular slit diaphragm of rats, [1, 10, 12] and made a rough estimates of R to be 2-10 nm. The space between fibers are assumed to be of the same range. As mentioned in Chapter 3, the averaged fluid velocity through the slit diaphragm is $3\text{x}10^{5}$ m/s. With r_s of myoglobin being 2 nm, its diffusivity in an unbounded fluid is approximately 10^{-10} m^2/s. The calculation of the solute concentration (and hence the sieving coefficient) across the slit diaphragm is outlined in Chapter 3.

In the GBM, the averaged fluid velocity within the hydrogel is assumed to be $4\text{x}10^{-6}$ m/s (a value typically used as an estimate for fluid velocity in GBM of rat; it is almost 10 times smaller than the averaged value in the slit diaphragm in keeping with fractional area of glomerular slit is 0.11). The diffusive hindrance factor (K_d) is calculated using Eq. (4.13). For the convective hindrance factor (K_c), we used the value reported for ΦK_c of ficoll in an isolated GBM [25] which is approximately 0.24. The volume fraction of the fibers is 0.1.

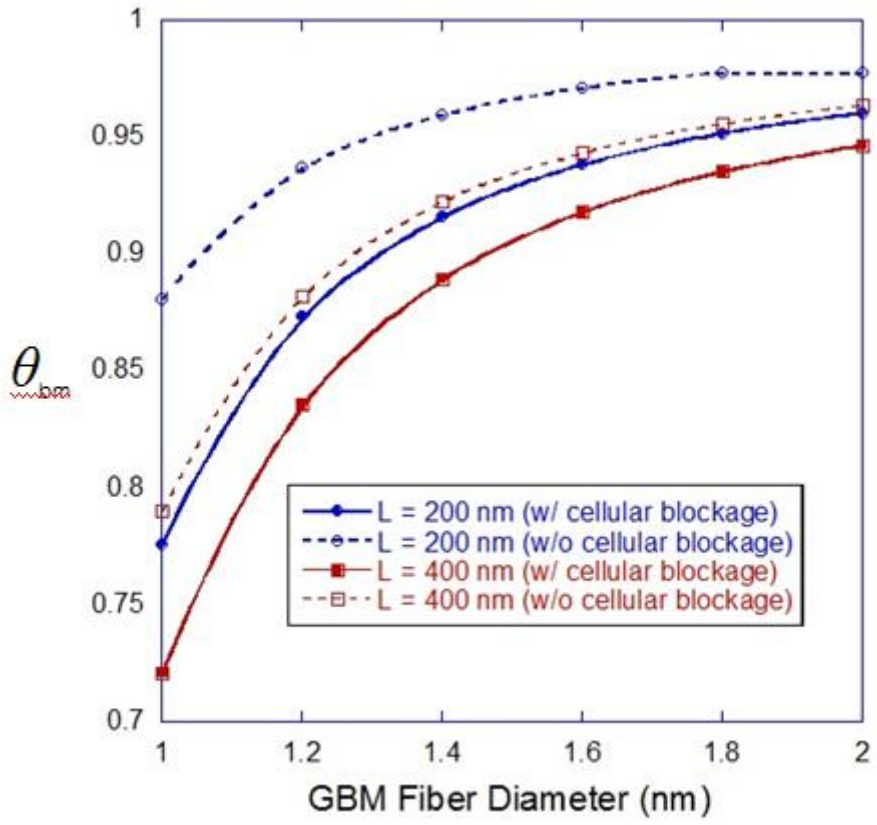

Figure 4.4 Numerically calculated glomerular sieving coefficient of myoglobin as a function of GBM fiber radii employed in the calculation. Results are plotted for H = 200 nm (circles) and 400 nm (squares). R = 10 nm and so is the half-width of the gap between the two adjacent fibers in the slit diaphragm.

Fig. 4.4 is the numerically calculated sieving coefficient through GBM of myoglobin as a function of GBM fiber diameter employed in the calculation. Based on results in Section 4.1, we decide to focus on the value of fiber diameter in the range of 1-2 nm. (r_f = 0.5 - 1 nm.) Results are plotted for two values of GBM thickness: H = 200 and 400 nm. The solid lines are result calculated with an inclusion of GBM cellular blockage and the dashed line are results calculated without an inclusion of GBM cellular blockage by simply using Eq.(4.3). As can be expected, inclusion of the cellular blockage of the GBM surface in the calculation reduces the sieving coefficient of myoglobin. The reported values of sieving coefficient of electrically neutral myoglobin and ficoll of the same sizes fall in the range of

0.7-0.8 nm. It can be seen from Fig. 4.4 that the value of GBM fiber diameter that give the result in this range is 1 nm (r_f = 0.5 nm), which is the diameter of the GAG chain of the proteoglycan, similarly to the comparison between the analytical solution and the sieving coefficient through an isolated GBM of solutes with r_s = 2 nm shown in Fig 4.2 and 4.4 Even though the volume fraction of the fine and coarse fibers, namely GAG chains and type IV collagens, are not known, Deen et al. [4] suggested from the reported values of the Darcy permeability of the GBM that the ratio between the volume fractions of the two types of fiber should be 1:1. With the fiber radii of GAG chains being 7 times smaller than those of the collagens and assuming that both fibers are cylindrical, equal volume fraction would means that the number of GAG chains presented in the GBM is 49 times that of the collagens. Myoglobins, being relatively small macromolecules, have much more chance at encountering and having a hydrodynamic interaction with the GAG chains than the collagens.

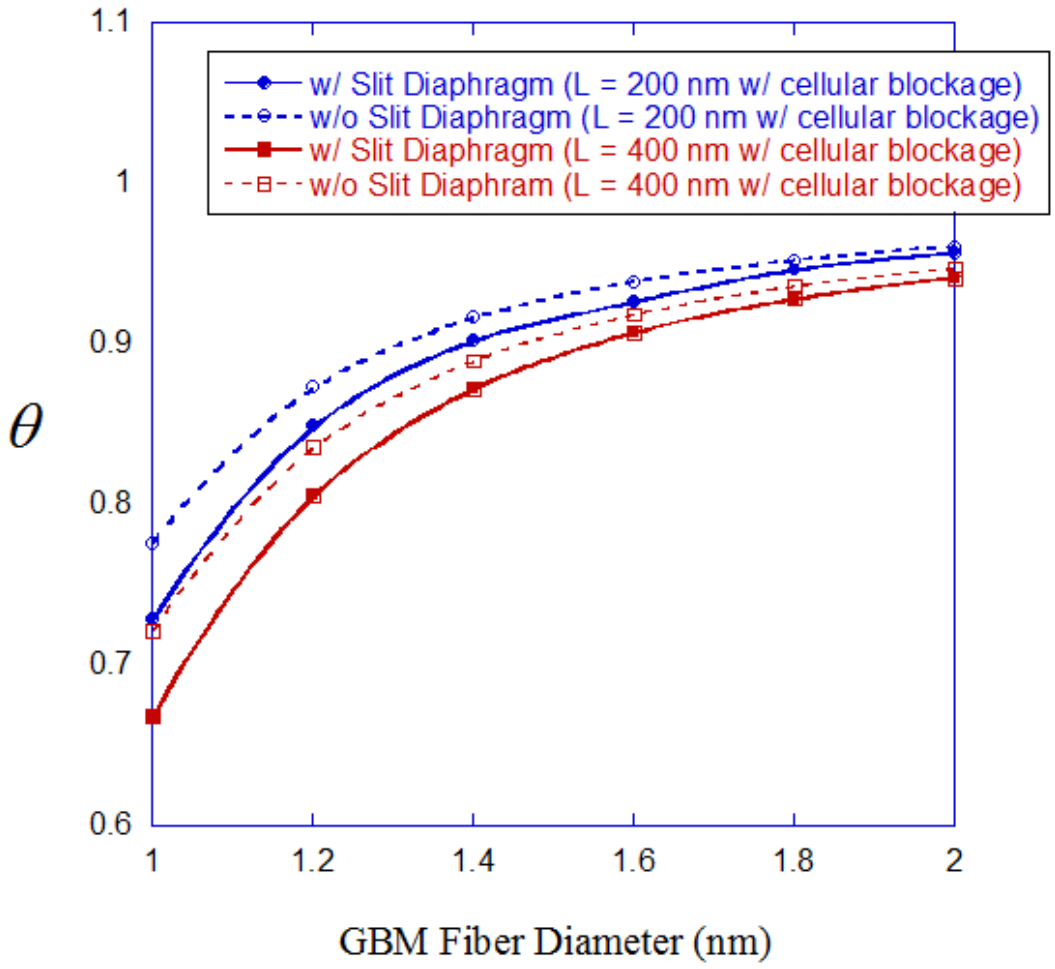

Figure 4.5 Numerically calculated glomerular sieving coefficient of myoglobin as a function of GBM fiber radii employed in the calculation. Presented above are the overall sieving coefficient with the slit diaphragm (solide lines) and without the slit diaphragm (dashed lines). Results are plotted for H = 200 nm (circles) and 400 nm (squares). R = 10 nm and so is the half-width of the gap between the two adjacent fibers in the slit diaphragm.

As shown in Fig. 4.5, the contribution on the overall sieving coefficient of spherical solute with r_s= 2 nm was determined. The numerically calculated glomerular sieving coefficient of myoglobin is presented as a function of GBM fiber diameter employed in the calculation. Results are plotted for two values of GBM thickness: H = 200 and 400 nm. The solid lines are the overall sieving coefficient calculated from a

product of sieving coefficients for the GBM and the epithelial slit diaphragm. The dashed line, on the other hand, are results calculated by setting the overall sieving coefficient equal to that of the GBM only and completely neglecting the sieving coefficient of solutes through the slit diaphragm. Neglecting the presence of the slit diaphragm reduces the overall glomerular sieving coefficient by 6-7%.

CHAPTER V

Summary and Conclusion

This research focuses on developing a mathematical model describing contributions of the glomerular basement membrane (GBM) and the slit diaphragm regarding size-selectivity of electrically-neutral molecules across the glomerular capillary wall, emphazing on the transport of myoglobins. The overall sieving coefficient (θ) of the glomerular capillary wall for myoglobin is approximated as the product of the sieving coefficient across GBM and through the slit diaphragm. For the slit diaphragm, force coefficient tensor as well as the hindrance factor tensor are calculated and employed in solving the convection diffusion equation. Likewise, for GBM, the convection diffusion equation are solved after determine the appropriate transport hindrance factors and other transport parameters are determined. The overall sieving coefficient of myoglobin is then compared with experimental.

The epithelial slit is modeled as a row of infinitely-long cylindrical fibers. Force coefficients are calculated from the hydrodynamic drag on a moving sphere in quiescent fluid, and that on a stationary sphere immersed in a passing flow, using COMSOL Multiphysics and, in the region where mesh generation proves to be a problem, results from lubrication theory of Falade and Brenner [23]. The fact that results of Falade and Brenner [23] are employed in the calculation implies that the spherical solute must be small compared to the gap between adjacent fibers ($r_s \le 0.3L$). For that range of molecular sizes, the effect of the coupling between translational and rotational motions on the force coefficients proves to be negligible. Diffusive and convective hindrance factor tensors are then determined, and the steady-state convection-diffusion equation are solved in order to obtain the solute concentration, and the solute sieving coefficient for the slit diaphragm. A plot of sieving coefficient for the slit diaphragm as a function of the Peclet number has a minimum: a result of concentration drop in the vicinity of the row of fibers caused by convection being balanced by a solute polarization upstream from the row of cylinders.

GBM, a second layer, is believed to be a hydrogel consisting of approximately 90% water and 10-11% fibers: mainly type IV collagen ($r_f = 3.5\,\text{nm}$) and proteoglycan with a protein core and glycoaminoglycan (GAG) chain ($r_f = 0.5\,\text{nm}$). A steady-state convection-diffusion equation is solved in order to determine the sieving coefficient for the GBM. Numerical calculations done with fiber radii assumed to be in the range of 0.5 - 1 nm yields sieving coefficient that is close to sieving coefficient of ficolls obtained from ultrafiltration through an isolated GBM with discrepancy between the numerical and experimental results being less than 15%. Sieving coefficient calculation done with diffusive hindrance factor (K_d) obtained from assuming that the GBM is a fibrous media with cylindrical fibers of uniform size gives results that are slightly closer to experimental data than the calculation done with K_d determined from assuming that the GBM is a Brinkman medium. Inclusion of the cellular blockage of the GBM surface in the calculation reduces the sieving coefficient of myoglobin by 8 - 11%.

The overall sieving coefficient of myoglobin is then determined from the product of its sieving coefficient through the slit diaphragm and that for the GBM. Calculation done assuming that the fiber radii are about 0.5 nm yields overall sieving coefficient that are close to sieving coefficient of myoglobin and ficolls obtained from the tissue-uptake techniques. With the gap between adjacent fibers in the epithelial slit diaphragm (L) assumed to be about 10 nm and so is the slit fiber radii (R), the absence of the slit diaphragm increases the sieving coefficient by only 6-7%. It seems that the GBM contributes significantly to sieving of myoglobin through the glomerular barrier, although it might still be too early to say that the contribution of slit diaphragm to transport of myoglobin is negligible, given that the values of L = 10 nm is the upper limit (a necessary condition given that r_s has to be smaller than $0.3L$ as discussed above). For smaller values of L, the sieving coefficient of myoglobin through slit diaphragm might be further reduced but it is likely not to be much smaller given that the Peclet number (Pe) falls into the range of 0.001-0.01. The slit diaphragm is likely to contribute significantly to the restriction of larger proteins such as albumin.

REFFERENCES

[1] Haraldsson, B., Nystrom, J., and Deen, W.M. (2008). Properties of the Glomerular Barrier and Mechanisms of Proteinuria**. Physiol Rev** 88: 451–487.

[2] Tryggvason, K, Wartiovaara, J. (2005). How does kidney filter plasma? **Physiology (Bethesda)** 20: 96-101.

[3] Deen, W.M. (2004). What determines glomerular capillary permeability? **J Clin Invest** 114: 1412-1414.

[4] Deen, W.M., Lazzara, M.J., and Myers, B.D. (2001). Structural determinants of glomerular permeability. **Am J Physics Renal Physiol** 281: F579-F596.

[5] Caulfield, J.P., and Farquhar, M.G. (1974). The permeability of glomerular capillaries to graded dextrans. Identification of the basement membrane as the primary filtration barrier. **J. Cell Biol.** 63: 883-903.

[6] Batsford, S.R., Rohrbach R., and Vogt, A. (1987). Size restriction in the glomerular capillary wall: importance of lamina densa. **Kidney Int.** 31: 710-717.

[7] Navar, L.G. (2009). Glomerular penmeability: a never-ending saga. **Am J Physiol Renal Physiol** 296: F1266-F1268.

[8] Tanner, G.A. (2009). Glomerular sieving coefficient of serum albumin in the rat: a two-photon microscopy study. **Am J Physiol Renal Physiol** 296: F1258-F1265.

[9] Rodewald, R., and Karnovsky, M.J. (1974). Porous substructure of the glomerular slit diaphragm in the rat and mouse. **J Cell Biol** 60: 423–433.

[10] Wartiovaara et al. (2004). Nephrin strands contribute to a porous slit diaphragm scaffold as revealed by electron tomography. **J. Clinical Invest** 114: 1475 -1483.

[11] Hora, K., et al. (1990). Three-dimensional study of glomerular slit diaphragm by the quick-freezing and deep-etching replica method. **Eur J Cell Biol** 53: 402–406.

[12] Drumond, M.C., and Deen, W.M. (1995). Hindered transport of macromolecules through a single row of cylinders: application to glomerular filtration. **J. Biomech. Eng**. 117: 414-422.

[13] Jeansson, M., and Haraldsson, B. (2003). Glomerular size and charge selectivity in the mouse after exposure to glucosaminoglycan-degrading enzymes. **J. Am. Soc. Nephrol.** 14: 1756-1765.

[14] Goldman, A.J., Cox, R.G., and Brenner, H. (1967). Slow viscous motion of a sphere parallel to a plane wall-II Couette flow. **Chem. Engng Sci** 22: 653-660.

[15] Happel, J., and Brenner, H. (1983). **Low Reynolds Number Hydrodynamics**. Netherlands: Martinus Nijhoff Publishers.

[16] Deen, W.M. (1987). Hindered Transport of Large Molecules in Liquid-Filled Pores. **AIChE J** 33: 1409-1425.

[17] Dechadilok, P., and Deen, W.M. (2006). Hindrance factors for diffusion and convection in pores. **Ind Engin Chem Res** 45: 6953-6959.

[18] Phillips, R.J., Deen, W.M. and Brady, J.F. (1989). Hindered transport in fibrous membranes and gels. **AIChE J** 35: 1761-1769.

[19] Phillips, R.J., Deen, W.M. and Brady, J.F. (1990). Hindered transport in fibrous membranes and gels : Effect of solute size and fiber configuration. **J. Colloid Interface Sci**, 139(2): 363-373.

[20] Phillips, R.J. (2000). A Hydrodynamic Model for Hindered Diffusion of Proteins and Micelles in Hydrogels. **Biophys J** 79: 3350-3354.

[21] Ganatos, P., Pfeffer, R., Weinbaum, S. (1980). A Strong Interaction Theory for the Creeping Motion of a Sphere between Plane Parallel Boundaries Part 2. Parallel Motion. **J. Fluid Mech** 99: 755-783.

[22] Cox, R.G., and Brenner, H. (1967). The slow motion of a sphere through a viscous fluid towards a plane surface-II Small gap widths, including inertial effects. **Chemical Engineering Science** 22: 1753-1777.

[23] Falade, A., and Brenner, H. (1988). First-order wall curvature effects upon the Stokes resistance of a spherical particle moving in close proximity to a solid wall. **J. Fluid Mech** 193: 533-568.

[24] Kongoup, P., and Dechadilok, P. (2013). Transport of Macromolecules through Glomerular Basement Membrane. **Siam Physics Congress 2013**, Thailand.

[25] Bolton, G.R., Deen, W.M., and Daniels, B.S. (1998) Assessment of the charge selectivity of glomerular basement membrane using Ficoll sulfate. **Am J Physiol Renal Physiol** 274: F889–F896.

[26] Lund, U., Rippe, A., Venturoli, D., Tenstad, O., Grubb, A.,and Rippe, B. (2003). Glomerular filtration rate dependence of sieving of albumin and some neutral proteins in rat kidneys. **Am J Physiol Renal Physiol** 284: F1226–F1234.

[27] Wolgast, M., and Ojteg, G. (1988). Electrophysiology of renal capillary membranes: gel concept applied and Starling model challenged. **Am J Physiol Renal Fluid Electrolyte Physiol** 254: F364–F373.

[28] Oliver, J.D., Simons, J.L., Troy, J.L., Provoost, A.P., Brenner, B.M., and Deen W.M. (1994). Proteinuria and impaired glomerular permselectivity in uninephrectomized fawn-hooded rats. **Am J Physiol Renal Fluid Electrolyte Physiol** 267: F917–F925.

[29] Edwards, A., Daniels, B.S., and Deen, W.M. (1997). Hindered transport of macromolecules in isolated glomeruli. II. Convection and pressure effects in basement membrane. **Biophys J** 72: 214–222.

[30] Amsden, B., (1998). Solute diffusion within hydrogel. Mechanisms and models. **Macromolecules** 31: 8382-8395.

APPENDIX

Lubrication Theory

The force coefficients are position-dependent. If the row of cylinders is not presented, **f** and **g** would equal an identity tensor. Both **f** and **g** are computed numerically overall the interested domain. But when the gap widths between sphere and cylinder is sufficiently small or the gap width tends to zero, the numerical results seem not to be correct. One way to solve this issue is using the lubrication theory to find the force coefficients in the asymptotic limit region.

A-1 Sphere Moving Near a Circular Cylindrical Wall

Falade and Brenner [23]introduce the expression for force and torque in asymptotic limit by including effect from surface curvature.

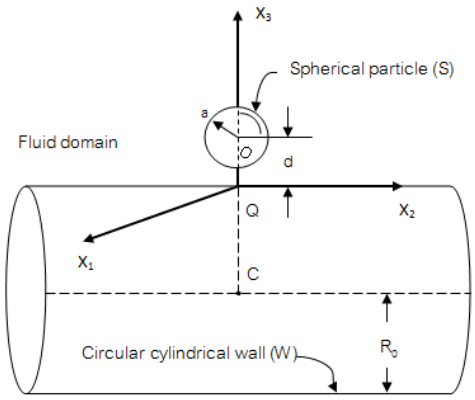

Figure A-1 Definition sketch [23]

Falade and Brenner [23] describing motion of a sphere near arbitrary curve wall by the position-dependent translational, rotational and coupling resistance dyadics ${}_{0,1}K^{t}$, ${}_{0,1}K^{r}$ and ${}_{0,1}K^{c}$ respectively. All these dyadics involve with scalar resistance functions a, b, c, d, e, A, B, C, D, E, F, G and H which presented in tabular form as a function of d/a.

The zero-order resistance dyadics can be written as,

$$ {}_0K^t = (I - i_3 i_3)a + i_3 i_3 b \tag{a5} $$

$$ {}_0K^r = (I - i_3 i_3)c + i_3 i_3 d \tag{a6} $$

$$ {}_0K^c = \varepsilon . i_3 e \tag{a7} $$

where $I = i_1 i_1 + i_2 i_2 + i_3 i_3$ and $\varepsilon = i_1 i_2 i_3 - i_1 i_3 i_2 + i_2 i_3 i_1 - i_2 i_1 i_3 + i_3 i_1 i_2 - i_3 i_2 i_1$ and the five scalar resistance coefficient *a, b, c, d* and *e* is a function of a/d.

When including the curvature effect yields the first-order resistance dyadics which can be written as,

$$ {}_1K^t = \alpha_1 (i_1 i_1 A + i_2 i_2 B + i_3 i_3 C) + \alpha_2 (i_1 i_1 A + i_2 i_2 B + i_3 i_3 C) \tag{a8} $$

$$ {}_1K^r = \alpha_1 (i_1 i_1 D + i_2 i_2 E + i_3 i_3 F) + \alpha_2 (i_1 i_1 E + i_2 i_2 D + i_3 i_3 F) \tag{a9} $$

$$ {}_1K^C = -\alpha_1 (i_1 i_2 G - i_2 i_1 H) - \alpha_2 (i_1 i_2 H - i_2 i_1 G) \tag{a10} $$

where α_1 and α_2 are the curvature parameters. For a circular cylindrical geometry when sphere is located outside of the cylinder α_1=-1 and α_2=0. The eight scalar resistance coefficients *A, B, C, D, E, F, G* and *H* are also depend on a/d.

Eq. (a5) to Eq. (a10) can be represented in matrix form with the non-dimensional force and torque;

$$ -\begin{bmatrix} F_1 \\ F_2 \\ F_3 \\ T_1 \\ T_2 \\ T_3 \end{bmatrix} = \begin{bmatrix} K_{11}^t & \cdot & \cdot & \cdot & -\frac{4}{3}K_{21}^c & \cdot \\ \cdot & K_{22}^t & \cdot & \frac{4}{3}K_{12}^c & \cdot & \cdot \\ \cdot & \cdot & K_{33}^t & \cdot & \cdot & \cdot \\ \cdot & K_{12}^c & \cdot & K_{11}^r & \cdot & \cdot \\ -K_{21}^c & \cdot & \cdot & \cdot & K_{22}^r & \cdot \\ \cdot & \cdot & \cdot & \cdot & \cdot & K_{33}^r \end{bmatrix} \begin{bmatrix} U_1 \\ U_2 \\ U_3 \\ \Omega_1 \\ \Omega_2 \\ \Omega_3 \end{bmatrix} \tag{a11} $$

in which

$$K_{11}^{t} = a - A\beta + O(\beta^2), \quad K_{22}^{t} = a - B\beta + O(\beta^2), \; K_{aa}^{t} = b - C\beta + O(\beta^2) \tag{a12}$$

$$K_{11}^{r} = c - D\beta + O(\beta^2), \; K_{22}^{r} = c - E\beta + O(\beta^2), \; K_{aa}^{r} = d - F\beta + O(\beta^2) \tag{a13}$$

$$K_{12}^{C} = e + G\beta + O(\beta^2), \; K_{21}^{r} = e + H\beta + O(\beta^2) \tag{a14}$$

and $\beta = a/R_0$ (where a = sphere radius, R_0 = cylinder radius)

General from of lubrication expression follow by Falade and Brenner [23]

$$f_{xx} = f_u \cos^2\theta + f_L \sin^2\theta \tag{a15}$$

$$f_{zz} = f_u \sin^2\theta + f_L \cos^2\theta \tag{a16}$$

$$f_{xz} = f_{zx} = f_u \cos\theta \sin\theta - f_L \cos\theta \sin\theta \tag{a17}$$

where $\sin\theta = \dfrac{x}{d+1}$, $\cos\theta = \dfrac{(\frac{L}{2}+1) - z}{d+1}$ and d is a distance between sphere center and cylinder surface.

In our coordinate we use $f_{ll} = K^t_{11}$ and $f_L = K^t_{33}$ followed Falade and Brenner [23] notation.

Table A-1 Force coefficient for a spherical particle moving near a circular cylindrical wall.

a	d	f_{ll}	f_L
0.1	1	0.99632	1.09807
0.1	0.5	1.06262	1.25685
0.1	0.3	1.16333	1.51621
0.1	0.2	1.31821	2.03294
0.1	0.18	1.38001	2.28632
0.1	0.16	1.46748	2.70257
0.1	0.15	1.52811	3.00799
0.1	0.14	1.59235	3.51917
0.1	0.12	1.84182	5.90761
0.1	0.11	2.09367	10.58295
0.1	0.1075	2.20186	13.78692
0.1	0.105	2.35981	19.90862
0.1	0.1025	2.64948	38.32768
0.1	0.1005	3.32435	183.9621

BIOGRAPHY

Mr. Piya Phalakhoj was born on August 25, 1982 in Yala, Thailand. He received the bachelor's degree from the Department of Physics, Faculty of Science, Thaksin University in 2005. He received the graduate diploma in Teaching from Department of Curriculum and Teaching, Faculty of Education, Thaksin University in 2006. He was admitted to the master's degree Program of Physics, Faculty of Science, Chulalongkorn University and completed the program in 2012. Now, he is a science teacher at Khanom Pitaya School, Nakhon Si Thammarat.

Proceeding Publication:

2011 P. Phalakhoj and P. Dechadilok. Hindered diffusion of spherical particles through a single row of parallel fibers. The 23rd National Graduate Research Conference. Nakorn Ratchasima, Thailand (December 23-24, 2011).